# THE $Li^7(p,\gamma)Be^8$ REACTION AND STUDIES IN PHOTODISINTEGRATION.

by

B. Mainsbridge,

Research School of Physical Sciences.

A dissertation submitted to the Australian National University for the degree of Doctor of Philosophy.

April, 1960.

# PREFACE.

This thesis is an account of experimental studies of the $Li^7(p,\gamma)Be^8$ reaction and its use as a gamma ray source in photodisintegration studies.

The investigations reported have been carried out independently but I wish to express my indebtedness to Mr. I.F. Wright and Dr. T.R. Ophel for the introduction to the techniques of their experiments in the photodisintegration of inorganic scintillators, and again to Mr. Wright for his supervision of this portion of my work.

I wish to thank Mr. D.S. Gemmell and Mr. I.F. Wright for helpful advice in the design of the $Li^7(p,\gamma)Be^8$ experiment and thanks are especially due to Dr. F.C. Barker and Miss E. Bradford of the Department of Theoretical Physics for valuable discussions during the course of the experiment.

The efficient maintenance and operation of the 1.2 Mev Cockcroft-Walton accelerator by Mr. N.F. Bowkett and Mr. H. Owen are gratefully acknowledged.

The whole of this work was carried out on a scholarship awarded by the Australian Atomic Energy Commission.

Some of the work presented in this dissertation is to be reported in the following journals:

1. "Composition of the $Li^7(p,\gamma)Be^8$ radiation from $E_p$ = 200 to 1100 Kev."

   Australian Journal of Physics 13 No.2.(1960).

2. "The Angular Distributions of the $Li^7(p,\gamma)Be^8$ Radiation from $E_p$ = 200 to 1100 Kev."

   Submitted to Nuclear Physics.

No part of this Thesis has been submitted for a degree at any other University.

B. Manisbridge.

CONTENTS.

# INTRODUCTION.

In the investigation of the absorption (or emission) of a gamma ray by a nucleus, a number of nuclear models have been proposed which can describe the process. A collective model of Goldhaber and Teller (Go 48) is a classical hydrodynamic model which assumes the protons to be moving in opposite directions to the neutrons in a nucleus, the gamma ray energy being stored in the form of a dipole vibration. This is essentially a compound nucleus description of absorption. In the model of Wilkinson (Wi 56) which is based on the independent particle model, a nucleon absorbs the gamma ray energy and moves to a higher shell, eventually sharing its energy by collision with other nucleons or escaping from the nucleus before this energy distribution can take place.

In the description of the emission of nucleons in photonuclear reactions, it appears from the Wilkinson theory that two processes are possible, direct emission of a nucleon immediately after the absorption of a gamma ray or the formation of a compound nucleus and the eventual evaporation of nucleons whose energy distribution can be calculated from the

statistical model. The energy distribution of the reaction products which have been measured suggest that the compound nucleus picture can account for the general energy distribution but the yield of high energy particles is significantly larger than the predictions (Di 50, By 51) and there is the possibility of both direct and compound nucleus mechanisms.

Both processes appear to have regions of validity which are determined by the mass number of the nucleus or the excitation energy involved. Compound nucleus formation is the main process for heavier nuclei at low energies and for lighter nuclei, both compound nucleus and direct transitions have been observed. For high energy photon absorption, direct transitions appear to be dominant.

From the experimental point of view, the measurement of photonuclear reactions is difficult. Because of the continuous energy spread of bremsstrahlung from betatrons and electron synchrotrons, excitation functions are measured by varying the end point energy, and the yield for each energy interval is obtained by a difference method. Results from various laboratories relating to the same nucleus are not in general agreement and beside bremsstrahlung

experiments, two methods of approach can be used to extend the field of measurement.

1. The cross sections of photon induced reactions have been measured using monochromatic radiation from proton capture in light nuclei. The most commonly used radiation has been the $Li^7(p,\gamma)Be^8$ reaction at the 441 Kev resonance.

2. The $(\gamma,p)$ and $(p,\gamma)$ reaction cross sections are related through the principle of detailed balance (Be 37) and it is possible to investigate the inverse $(p,\gamma)$ reactions to provide data for the interpretation of photonuclear reactions. (Ma 56, Ge 59, Go 59, Wi 59).

Both $(\gamma,p)$ and $(p,\gamma)$ reactions must be considered as fields of investigation whose ranges have been limited by technology; the first by the need for a variable energy, monochromatic gamma ray source and the latter by the need for well-resolved proton beams above 5 Mev in energy. The relatively low cross sections for these processes require detectors with high efficiency, good energy resolution and with low sensitivity to background. It is substantially true that only the general features of many of these reactions are known and a higher precision in measurement is required before any nuclear model can be

rigorously compared with experiment.

The investigations presented below are believed to include a number of refinements which have not been used extensively in earlier investigations.

In part A is reported the measurement of the angular distribution of the radiation from the $Li^7(p,\gamma)Be^8$ reaction in the proton energy range at present available in this laboratory. Using a large NaI(Tl) crystal, it has been possible to study separately the two gamma rays emitted and establish a marked difference in their behaviour in the neighbourhood of the 441 Kev and 1030 Kev resonances.

Part B describes the use of this radiation to investigate the $Na^{23}(\gamma,p)$ $Ne^{22}$ and $Br^{79,81}(\gamma,p)$ $Se^{78,80}$ reactions using thin inorganic scintillators as both target and detector. By this technique, it is possible to detect the reaction products with good resolution in the presence of a high gamma ray flux.

# PART A.

# The $Li^7(p,\gamma)Be^8$ Reaction.

## Chapter I.

a well-defined beam energy and thin targets. As a result, yields are low and background radiation from competitive reactions can be high. While these effects can be reduced by using energy sensitive detectors, many investigations have been hindered by the use of gamma ray spectrometers with limited resolution. Significant improvements in the accuracy of measurement have come with the advent of the pair spectrometer and the sodium iodide scintillation counter.

The excitation function of proton capture radiation generally includes a number of sharp resonances in the first few Mev of proton energy. These correspond to unique states in the compound nucleus with properties which can be determined from the level widths, angular distributions and intensity ratios of the gamma rays emitted at the resonance. At higher proton energies, the excitation function generally passes through a broad maximum which is believed to be the inverse of the giant resonance in photodisintegration.

Current theory suggests that radiative capture may proceed by way of the compound nucleus or capture of a proton into a bound level of the residual nucleus, accompanied by the emission of the

excess energy in the form of gamma ray quanta. For the lightest nuclei where the levels are widely separated, direct proton capture appears to be dominant as in $H^2(p,\gamma)He^3$ (Wi 52) and $H^3(p,\gamma)He^4$ (Fl 51). The excitation function of the latter reaction has no resonances at low excitation energies and the cross section rises steadily with proton energy (Pe 55).

The interest in the $Li^7(p,\gamma)Be^8$ reaction, apart from its use as a source of monochromatic radiation for photodisintegration studies, arises from the suggestion by Wilkinson (Wi 54) that it proceeds by way of compound nucleus and direct proton capture mechanisms. The large amount of experimental information on this reaction has been reviewed by Ajzenberg-Selove and Lauritsen (Aj 59) which for completeness is summarised below. As studies have been hampered by the difficulties inherent in gamma ray spectroscopy, the detection methods are discussed in the following sections so that the data may be critically evaluated before presenting the current work.

1.1. Excitation Function.

The $Li^7(p,\gamma)Be^8$ reaction is resonant at proton energies of 441 Kev (Bo 48), 1.03 Mev (Kr 54, Pr 54) and 2.1 Mev (Pr 54, Sw 55, Ne 57) corresponding

to levels in $Be^8$ at 17.64, 18.15 and 19.1 Mev. The 441 Kev resonance is 12 Kev wide and has a peak cross section of 6.0 mb. (Fo 49) while the 1.03 and 2.1 Mev resonances are much weaker and have widths of about 168 and 400 Kev respectively. Immediately above the 441 Kev resonance, the cross section is larger than can be explained by the resonance "tail" (Bo 48, Wi 54) and the two weak resonances are superimposed on a non-resonant background which increases slowly with proton energy, going through a broad maximum at 5.8 Mev (Ge 59).

1.2. Composition of the Radiation.

The radiation includes gamma rays of energy $(17.2 + 7/8\ Ep)$ and $(14.3 + 7/8\ Ep)$ Mev corresponding to transitions to the ground state and the first excited states of $Be^8$.† The relative intensities of the two gamma rays vary with proton energy and the 14.8 Mev gamma ray is approximately 2 Mev broad (Wa 48).

It is possible that there are other gamma rays present with an intensity of about 5% of the

---

† For convenience, the two gamma rays will be referred to in the text by their energies at the 441 Kev resonance, 17.6 and 14.8 Mev respectively.

total radiation. Evidence for these is discussed in section 2.

Angular correlation measurements at the 441 Kev resonance have shown the 17.6 Mev gamma ray to be magnetic dipole (M1) (De 54) and the 14.8 Mev gamma ray to be M1 + E2 (Bo 56).

1.3. Assignments to the Levels of $Be^8$ up to 18.15 Mev.

Alpha particles from the disintegration $Be^8 \rightarrow 2\alpha$ have been observed from the ground state and first excited state (2.9 Mev) of $Be^8$ (Jo 53, Bu 50) and this requires the two levels to have even parity and even angular momentum (J). As in the case of most even-even nuclei, the ground state and the first excited state of $Be^8$ are believed to be $J = 0^+$ and $2^+$ respectively. This is confirmed by the work of Devons and Goldring (De 54) and of Boyle (Bo 56).

The observed M1 and M1 + E2 character of the 441 Kev resonance radiation requires the 17.64 Mev level of $Be^8$ to have even parity and an angular momentum of 1. No $\alpha$ particle break up from this level has been observed and the odd J value is consistent with this fact.

Investigation of the radiation from the 1030 Kev resonance has not been extensive and no conclusions about the spin and parity of the 18.15 Mev level of

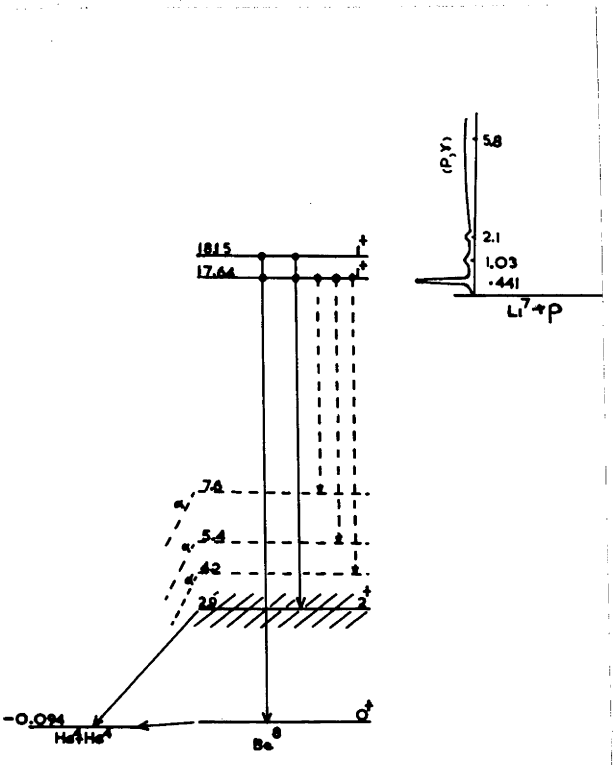


Fig. 1.1. Energy levels of $Be^8$

$Be^8$ can be made from the experimental evidence available (Kr 54).

Assignments to the 17.64 and 18.15 Mev levels of $Be^8$ have been made independently from the investigations of the elastic scattering of protons where anomalies have been observed at the 441 and 1030 Kev resonances. (Wa 53a). An analysis of the data established both the 17.64 and 18.15 Mev levels to be $J = 1^+$ and formed by p wave protons with channel spins 1 and 2 in the ratio 1 to 5 (Li 53, Ch 53, Li 55). In other words the $J = 1$ states of $Be^8$ are formed with equal probability in their substates $J_z = 0, \pm 1$ and radiative transitions from the 17.64 and 18.15 Mev levels to the $2^+$ and $0^+$ levels of $Be^8$ would be isotropic.

The information on the energy levels of $Be^8$ of interest in a discussion of the $Li^7(p,\gamma)Be^8$ reaction up to Ep = 1100 Kev is summarised in Figure 1.1.

## 2. Gamma Radiation Detectors Used in Previous Investigations of the $Li^7(p,\gamma)Be^8$ Reaction.

The significance of experimental measurements of the radiation must be considered in the light of the characteristics and limits of the various detectors used in past investigations,

and although the following discussion is not exhaustive, the principle methods are reviewed in order to present those properties of the radiation which are in doubt or which have yet to be measured.

2.1. Photodisintegration.

The measurement of the total energy released in the photodisintegration of a nucleus by radiation from the 441 Kev resonance enables the calculation of the energy and composition of the radiation. Investigations of this type have been carried out with the $C^{12}(\gamma,3\alpha)$ and $Li^{7}(\gamma,t)He^{4}$ reactions.

a. Nuclear Emulsions.

Nabholz et.al. (Na 51, Na 52) irradiated nuclear emulsions with resonance radiation and examined the $C^{12}(\gamma,3\alpha)$ reaction stars in the emulsion. A plot of the number of stars as a function of the total energy of the three alpha particles revealed three groups corresponding to gamma rays of energy 17.6, 14.8 and 12.6 Mev. A comparison of the yields at four angles of observation showed the radiation to be isotropic. The experiment was one of the first to suggest the existence of a third gamma ray from the $Li^{7}(p,\gamma)Be^{8}$ reaction. The experiment was repeated by Goward and Wilkins (Go 52) who found the third gamma ray line to have an energy of 12.3 Mev. The

relative intensity of the three gamma rays was estimated from the variation of the cross section of the $C^{12}(\gamma,3\alpha)$ reaction between $E_\gamma$ = 12 Mev and 17.6 Mev and the intensity of the 12.3 Mev gamma ray has been estimated at 6% and 25% of the total radiation by Nabholz et al. and Goward et al. The wide variation in the results is presumably due to the disagreement in the measurements of the cross section in this energy range (Ti 55).

An experiment was performed by Titterton (Ti 53, 54) using emulsions loaded with $Li^7$. The $Li^7(\gamma,t)He^4$ reaction cross section changes more slowly than the $C^{12}(\gamma,3\alpha)$ reaction in this energy range and the former reaction should give a more accurate measurement of the intensity of the components. Again, three gamma rays were observed and the energy of the third line was found to be 12.5 Mev with an intensity of about 5% of the total resonance radiation.

b. Proportional Counters.

In the measurement of the $C^{12}(\gamma,3\alpha)$ cross section at $E_\gamma$ = 17.6 Mev, a proportional counter, filled with methane gas has been irradiated with resonance radiation (Ca 55). Evidence for the presence of a weak gamma ray at 12.5 Mev was obtained after correction for a high background in this energy

region. The result must be admitted with some reservations in view of the large errors in the measurement although a further investigation of $C^{12}(\gamma,3\alpha)$ in a nuclear emulsion reported in the same paper shows identical features about $E_\gamma$ = 12.5 Mev.

A comparison of the two investigations demonstrates the type of situation where the nuclear emulsion is still a useful, if tedious, instrument in investigating aspects of a reaction which are not clearly resolved by electronic detectors. The fact remains that the evidence for the existence of a third gamma ray depends almost entirely on the nuclear emulsion measurements. It is also true that if such a weak line were to exist, the resolution of the present generation of electronic detectors is not sufficient to resolve it clearly in the presence of the 14.8 and 17.6 Mev gamma radiation.

2.2. Alpha-particle Spectroscopy.

Even parity, even angular momentum levels of $Be^8$ can break up into two $\alpha$ particles, and $\alpha$ groups observed in coincidence with the $Li^7(p,\gamma)Be^8$ radiation would identify levels of $Be^8$ formed in a gamma ray transition.

While Inall and Boyle (In 54) were able to find $\alpha$ groups corresponding to levels of $Be^8$ at 4.09, 5.31 and 7.5 Mev, a more recent experiment using a gamma ray detector with improved resolution has produced a negative result (Ge 60) and gamma ray transitions to levels of $Be^8$, other than the ground state and the 2.9 Mev level remain in doubt. In the present work, no evidence for these weak gamma rays was found and they were assumed not to be present.

2.3. Geiger Counters.

Many of the early measurements of the radiation were made using Geiger Counters (Hu 40, Ta 46, Bo 48, Fo 49). These counters have a low efficiency for the detection of gamma rays and this can be improved by placing thin aluminium radiators in front of the detector to serve as a source of secondary electrons. In addition, the aluminium serves as an absorber to reduce the contributions from low energy radiation from scattered gamma rays and from the accelerator. The pulse output is independent of the energy of the radiation detected and gamma ray energies are obtained by measuring the range of secondary electrons produced in a radiator (Fo 48). While this method is not precise, it is satisfactory for the measurement of a single gamma

ray energy. In the case of the $Li^7(p,\gamma)Be^8$ radiation, the ranges of secondary electrons produced by the two gamma rays are similar. The method is not satisfactory for the measurement of the composition of the radiation and the intensity ratios reported by Tangen (Ta 46) and Devons and Hine (De 49) are in disagreement with measurements made with pair spectrometers.

Devons and Hine (De 49) have measured the angular distribution of the two unresolved gamma rays at $E_p$ = 440, 650 and 890 Kev by using two geiger counters in line with the target and in coincidence. An aluminium radiator was placed in front of the first counter and an aluminium absorber was placed between the first and second counters. The radiator and absorber thickness combined was large enough to minimise the contributions from scattered radiation and secondary electrons from the target housing. A second pair of counters was placed on the opposite side of the target and two separate angular distributions were measured simultaneously from the number of coincidences and the counting rate from a single thick-walled geiger counter monitor placed under the target housing.

The angular distribution of the radiation was found to be isotropic within 6% at the 441 Kev

resonance and at $E_p$ = 650 and 890 was found to be of the form $1 + a_1 \cos\theta + a_2 \cos^2\theta$.

By measuring the ratio of the intensity of the radiation at 15° and 145° to the proton beam, they found there was interference in the neighbourhood of the 441 Kev resonance between the resonance radiation and radiation of opposite parity.

2.4. Magnetic Pair Spectrometers.

Semi-circular pair spectrometers after the design of McDaniel, von Dordel and Walker (McD 47) have detected the 17.6 Mev gamma ray with 6% resolution (Wa 48, De 50). With this instrument, the gamma rays are collimated on to a thin radiator foil and a uniform magnetic field bends the electrons and positrons produced in the radiator through opposite directions into geiger counter detectors. A coincidence circuit records the arrival of pairs and from the position of the two detectors, the sum of the radii of curvature can be obtained to calculate the gamma ray energy (Wa 48).

A gamma ray spectrum is obtained by varying the magnetic field and plotting coincidences against magnetic field strength. Corrections have to be made for the dependence of the detector efficiency on gamma ray energy. The resolution is limited by

scattering in the converter and by the width of the defining aperture in front of the pair detectors. Good resolution requires thin converters and narrow apertures with a consequent low coincidence rate. For this reason, investigations of the $Li^7(p,\gamma)Be^8$ reaction with this instrument have generally required targets about 150 Kev thick to increase the yield. At the 441 Kev resonance, the high cross section would enable the use of thinner targets, but only Devons and Lindsey have used targets 10-20 Kev thick at this resonance (De 50). They found the intensity ratio of the 17.6 Mev to the 14.8 Mev component to be 2:1 at 0° and 90° to the proton beam, with an accuracy of 20%. Walker and McDaniel have also measured the ratio and found it to be 2 : 1 at the 441 Kev resonance and 0.66 at $E_p$ = 1.15 Mev (Wa 48).

The use of this instrument for the measurement of angular distributions has not been extensive and at $E_p$ = 500 and 1150 Kev, with thick targets, has been limited to three angles between 0° and 75°. The two gamma rays are isotropic at the lower energy while at 1.15 Mev, they are anisotropic and markedly different. (St. 51). The latter observation is one of the few indications that the angular distributions

of the two gamma rays may differ.

2.5. Scintillation Counters.

The advent of the sodium iodide crystal activated with thallium widened the field of gamma ray spectroscopy considerably. The advantages of the scintillator lie in its relatively small size, high efficiency, satisfactory resolution and high speed. The disadvantages include the production of multiple peaks for a monochromatic gamma ray as a result of the various absorption processes in the detector. A detailed discussion of the scintillation counter follows below and in this section, it is only necessary to review the use of this type of detector in the investigation of the $Li^7(p,\gamma)Be^8$ reaction.

It is unfortunate that most of the measurements have been performed with small NaI(Tl) crystals which do not resolve the 14.8 and 17.6 Mev gamma rays. However Campbell (Ca 56) has used a 1-1/2 in. diameter by 1-1/2 in. long NaI(Tl) crystal to measure the intensity of the two gamma rays at 90° to the proton beam between $E_p$ = 200 Kev and 650 Kev, after assuming the value of the intensity ratio of 1.7 at the 441 Kev resonance reported by Stearns and McDaniel (St 51). The poor resolution gave rise to large experimental

errors.

Angular distributions of the two gamma rays have been measured at the 441 Kev resonance with a similar crystal by Neuert and Retz-Schmidt (Ne 58) who claim them to differ. Six measurements have been made between 0° and 145° and the scatter of points in the forward direction throws doubt on their conclusions.

A 3 in. diameter by 3 in. long NaI(Tl) crystal has been used to measure the angular distributions from $E_p$ = 880 to 1240 Kev and they are of the form $1 + a_1 \cos\theta + a_2 \cos^2\theta$ (Kr 54). The two components were not resolved and the value of $a_2$ at $E_p$ = 880 is considerably higher than that measured by Devons and Hine at 890 Kev (De 49).

Investigations of the response of large NaI (Tl) crystals to high energy radiation (Ko 59, Fo 54) have shown the 14.8 and 17.6 Mev gamma rays to be partly resolved but no investigations have been reported beyond this observation.

2.6. Summary.

Most of the information on the $Li^7(p,\gamma)Be^8$ reaction has been obtained using detectors which do not resolve the two gamma rays.

At the 441 Kev resonance, the two components are approximately isotropic and this is consistent with the resonance being p wave with channel spins 1 and 2 in the ratio of 1 : 5 (De 50). The level assignments to the 1030 Kev resonance from the $Li^7(p,p)$ data are identical and predict isotropic angular distributions for $Li^7(p,\gamma)Be^8$ at this resonance. This is in disagreement with measurement (Kr 54). The contribution of the non-resonant background is considerable in this energy region and it is not known if the anisotropy is due to the resonance or the background. Wilkinson (Wi 54) has suggested the background to be from direct s wave proton capture to the ground state and first excited state of $Be^8$ and while this theory is sufficient to explain the magnitude of the cross section between the resonances, it would require the background to be isotropic, although a small contribution from d wave protons could account for the observed anisotropy. A further complication arises from the observation of Stearns and McDaniel (St 51) who found the angular distributions of the two components to be markedly different in this energy region. Apart from this measurement and those at the 441 Kev resonance, no angular distributions in which the two gamma rays are resolved

have been measured, and there is a need for a detailed investigation of this matter before the distributions can be interpreted unambiguously.

3.1. The Present Method.

The experiment was designed to measure the separate angular distributions of the 14.8 and 17.6 Mev gamma rays from proton capture in $Li^7$ in the energy range of the Canberra 1.2 Mev Cockcroft-Walton accelerator. The detector was a 5 in. diameter by 4 in. long NaI(Tl) crystal which, with suitable collimation, gave a resolution of 13% for the 17.6 Mev gamma ray. The angular distributions of this component $W(\theta)_{17.6}$ and of the unresolved gamma rays $W(\theta)_{14.8+17.6}$ were obtained directly from the pulse height distributions at each angle of observation. The angular distribution of the 14.8 Mev component $W(\theta)_{14.8}$ was obtained analytically from $W(\theta)_{17.6}$ and $W(\theta)_{14.8+17.6}$ using the value of the intensity ratio of the two components measured at $\theta = 90°$.

3.2. Presentation of Material.

Chapter II is devoted to a summary of the apparatus and experimental techniques used in the measurements and in Chapter III, the measurement of the variation of the intensity ratio of the two components with proton energy is described. The angular distributions of the two components are

presented in Chapter IV where it is seen that they differ markedly in the region of the 441 and 1030 Kev resonances. In Chapter V, the results are discussed and the conclusions are compared with present theories on the mechanism of the reaction.

# CHAPTER II.

INTRODUCTION.

This chapter is concerned with the experimental aspects of the investigation. In section I the apparatus, targets and detection methods are described. Section 2 is devoted to the properties of the spectrometer and the absorption process which gives rise to the pulse output from the photomultiplier. A brief investigation of the effect of collimator size on resolution is described and the pulse height distributions of the 17.6 and 14.8 Mev gamma rays are separated from the $Li^7(p,\gamma)Be^8$ spectra.

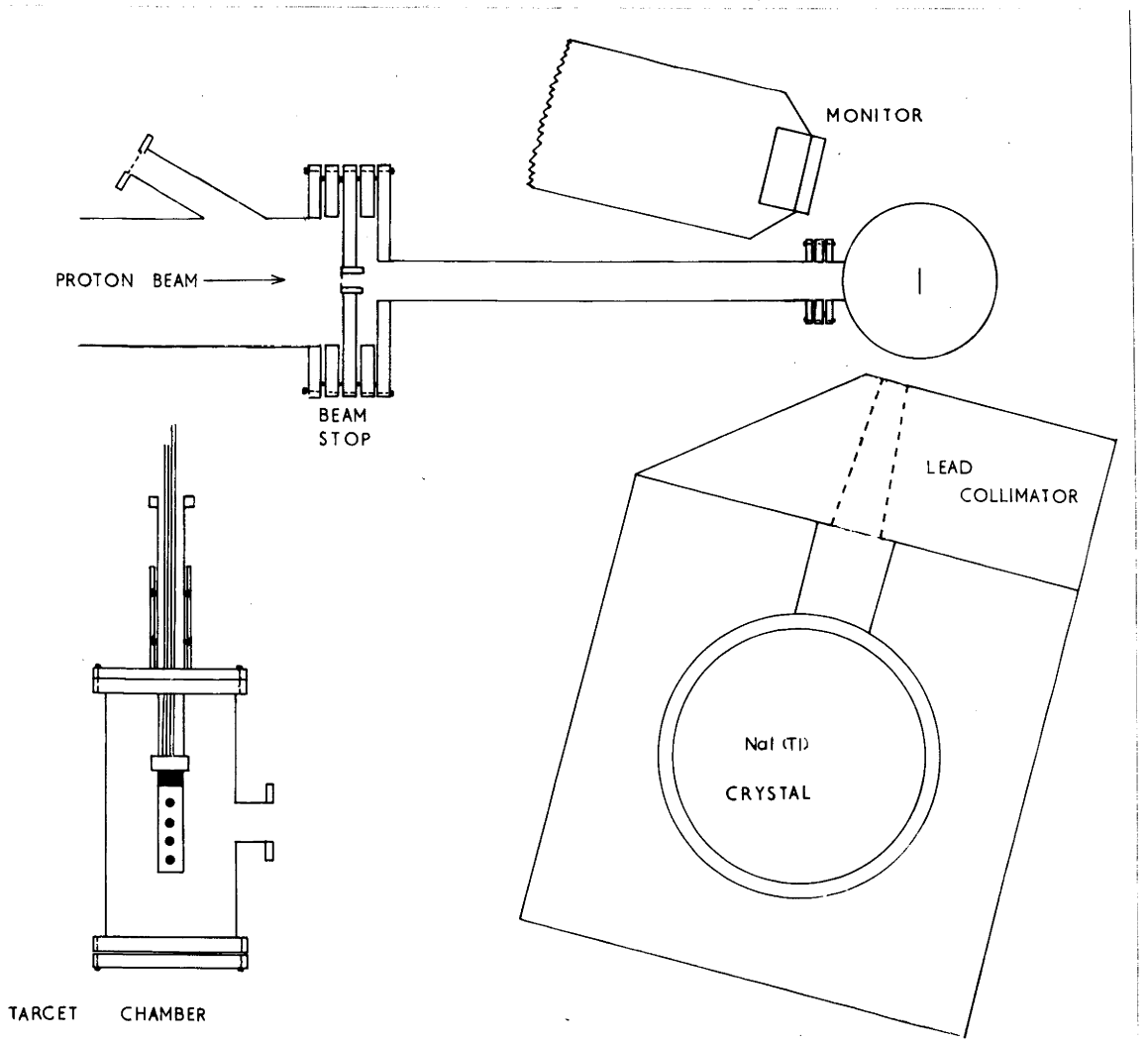


Fig. 2.1. Experimental arrangement.

1.1. Apparatus.

A diagram of the apparatus used in the experiment is shown in figure 2.1. The target chamber was a brass cylinder 5 in. high, 3 in. diameter with walls 1/8 in. thick, a perspex inspection window being included in the base.

The sodium iodide detector was mounted with the cylindrical axis vertical, in a 9 in. x 9 in. x 6 in. steel block which stood on a rotating table set so that the axis of rotation passed through the centre of the target. The gamma radiation was collimated into the crystal centre by a conical hole through a lead block, 3 in. thick. The collimator was tapered so that the detector observed, through a solid angle of 0.074 steradians, a 1/4 in. diameter spot at the target. The remaining five sides of the crystal mounting were not shielded with lead.

A 1-1/2 in. diameter by 1 in. NaI(Tl) crystal was used as a gamma ray monitor and set at -130°, 6 in. from the target.

1.2. Proton Beam.

The proton beam from the Canberra 1.2 Mev Cockcroft-Walton accelerator was analysed by a 90° deflecting magnet and was defined at the entrance to the magnet by a 1/4 in. slit and at the exit by the

jaws of the electronic voltage stabiliser set to a 1/4 in. gap. The emergent beam was focussed by strong focussing electrostatic lenses and deflected through a 45° analysing magnet and a 3/16 in. diameter aperture (beam stop) on to the target. The stop and the 3/16 in. diameter target spot defined the direction of the beam. The long path length of the protons defined the beam energy which was believed to be stable within 1 Kev.

Currents of 1 - 15μA. were used in the experiment and by adjusting the controls of the electrostatic lenses while watching the beam spot on the target it was possible to focus the beam to an 1/8 in. central spot. Under these sharp focus conditions, the beam stop current was limited to 0 - 4μA. Periodic checks on the spot position and focus were made during the measurements but few adjustments were necessary.

The machine was calibrated at the 340, 484, 672, 874 and 935 Kev resonances in the $F^{19}(p;\alpha,\gamma)O^{16}$ reactions.

1.3. Target Preparation.

Targets 5 to 20 Kev thick were deposited by evaporating natural lithium metal on to silver-plated brass backings 0.015 in. thick. Each backing was masked so that four targets, 3/16 in. in diameter and 3/8 in. apart were deposited as well as a 1/2in. by 1/4 in. rectangle of lithium, which was used to measure

the thickness of the deposit at the 441 Kev resonance. The backing material was originally of brass but earlier experiments in this laboratory, using thick lithium targets on copper, showed the backing material to become pitted because of the chemical interaction between the two elements. Small pits in the backing material can accumulate lithium metal and lead to variations in thickness over the target area. This effect can be troublesome when investigating the region above a sharp resonance with a thin target where small portions of the target may be thick enough to contribute some resonance radiation.

Pitting was less noticeable on the surface of silver backings and to minimise this effect, the brass backings were silver plated and were highly polished before each evaporation.

To prevent oxidation of the lithium after evaporation, the evaporator was filled with dry argon and the targets were transferred to the target chamber in an atmosphere of this gas. In the chamber, the target backing was screwed to a water-cooled holder which could be raised using a series of 3/8 in. spacers to position the target in the centre of rotation of the detector. Each target was changed after the measurement of one angular distribution.

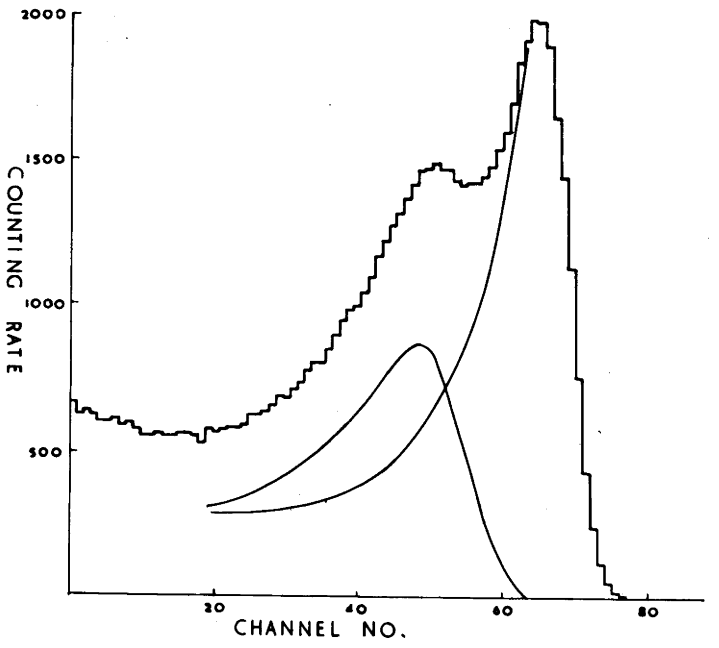


Fig. 2.2. Pulse height distribution of the $Li^7(p,\gamma)Be^8$ radiation detected by the 5 in. diameter x 4 in. long NaI(Tl) detector. ($E_p$ = 500 Kev, target 200 Kev thick, $\theta$ = 0°)

Because of the large number of targets employed, no attempt was made to measure an excitation function accurately, but a beam current integrator was used in the measurement of each target thickness at the 441 Kev resonance and to monitor the change of yield with running time. In 2 hours, at $E_p$ = 600 Kev and a current of 10 μA., the gradual accumulation of carbon on the target increased the thickness by 5 Kev, despite the use of liquid air traps, while after 3 to 4 hours, the yield began to fall off rapidly. For these reasons, the running time was limited to 3 to 4 hours for each target.

1.4. Electronics.

Scintillations in the 5 in. and 1-1/2 in. NaI(Tl) crystals were detected by a 5 in. Dumont 6364 and a 2 in. 6097 B E.M.I. photomultiplier.

The 5 in. phototube was surrounded by a mu-metal shield and the output was amplified by a Fairstein (Fa 56) non-overload amplifier and fed to a Hutchinson-Scarrott type 100 channel pulse height analyser biased at 6 Mev gamma ray energy. An examination of the pulse height distributions of the lithium gamma rays showed the gain of the system was stable within 1%.

Pulses from the monitor detector were amplified by a Higinbotham non-overload amplifier and fed

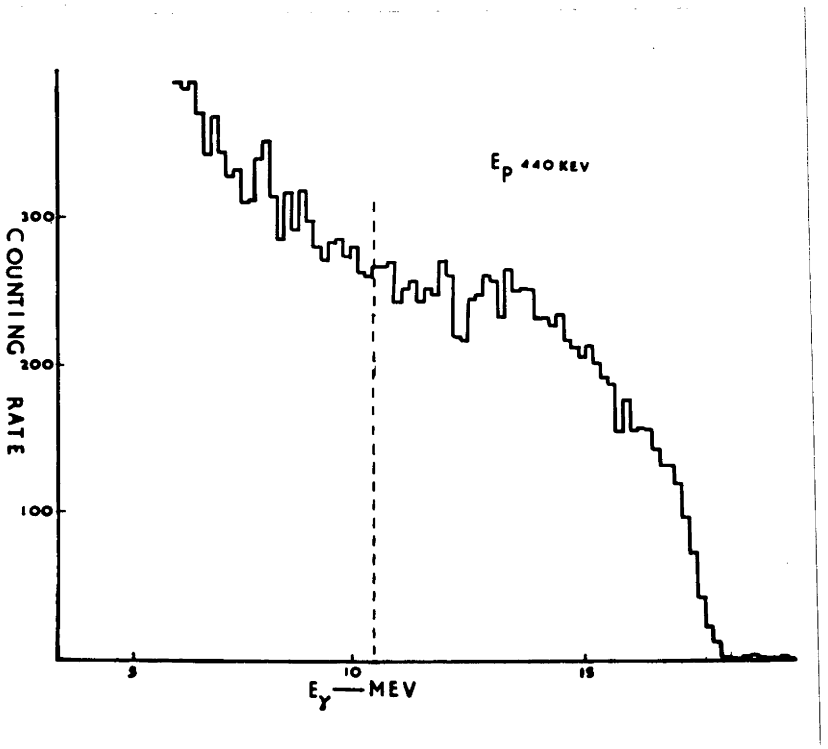


Fig. 2.3. Pulse height distribution of resonance radiation detected by the 1-1/2 in. diameter x 1 in. long NaI(Tl) monitor. The broken line shows the bias point on the scaling circuit.

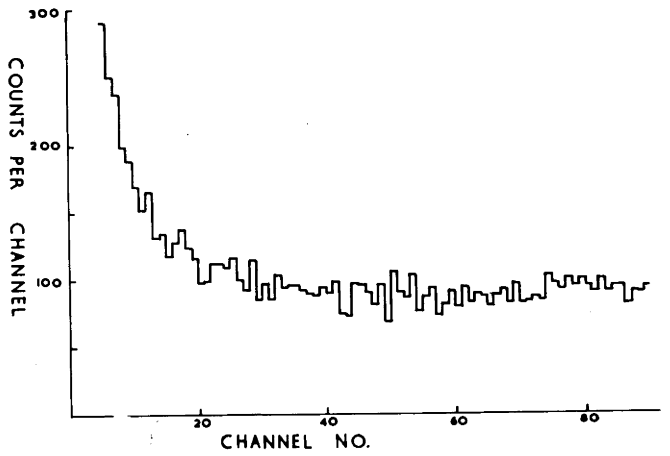


Fig. 2.4. Cosmic ray background for large crystal. Running time = 2 hours.

to a scaler with the discriminator set to count all events above $E_\gamma$ = 10.6 Mev. The bias point was calculated by measuring the pulse height of the 1.33 Mev gamma ray from $Co^{60}$ on the kicksorter set to the gain X10 scale. Gain shifts of more than 2% could be detected in this manner and the system was found to be stable within this limit. Figures 2.2 and 2.3 show typical spectra from the pulse height analysis of radiation from the 441 Kev resonance, detected by the large crystal and the monitor.

1.5. Background.

a. Cosmic Rays.

This background was measured by running the electronics with the accelerator switched off. Figure 2.4 shows a background obtained from the large crystal in two hours. In the energy region of interest in the experiment, the pulse height distribution was quite flat; the counting rate was constant and could be determined accurately. For the thin targets used, this background was as high as 10% of the reaction yield but the spectra and the monitor counts were easily corrected for this contribution.

b. Competitive Reactions.

Because of the sharp focus, the beam stop and the target were the only significant sources of radiation

from the accelerator. Gamma rays from the 6.1 and 7.1 Mev levels of $O^{16}$ in the $F^{19}(p;\alpha,\gamma)O^{16}$ reactions were detected but were eliminated by accepting the spectra above $E_\gamma$ = 8.5 Mev.

The variation of the background with angle of observation was investigated by raising the target from the beam path and allowing the beam to strike the back of the target chamber. It was found to be independent of the angle of observation beyond $E_\gamma$ = 8.5 Mev and entirely due to cosmic rays.

c. Scattering.

The apparatus included a considerable amount of heavy scattering material but the energy spectra from the large crystal suggested that most of the scattered gamma rays detected were of low energy and significant only below $E_\gamma$ = 8 Mev. The discriminator of the monitor scaler was set to count all events above $E_\gamma$ = 10.6 Mev and a check at the 441 Kev resonance showed the ratio of monitor counts to current integrator counts was independent of the position of the crystal mounting.

Section 2. The NaI(Tl) Spectrometer.

After considering the gamma ray absorption process, the factors affecting the resolution of the detector are obtained. The effect of collimator size on resolution is measured and the line shapes of the

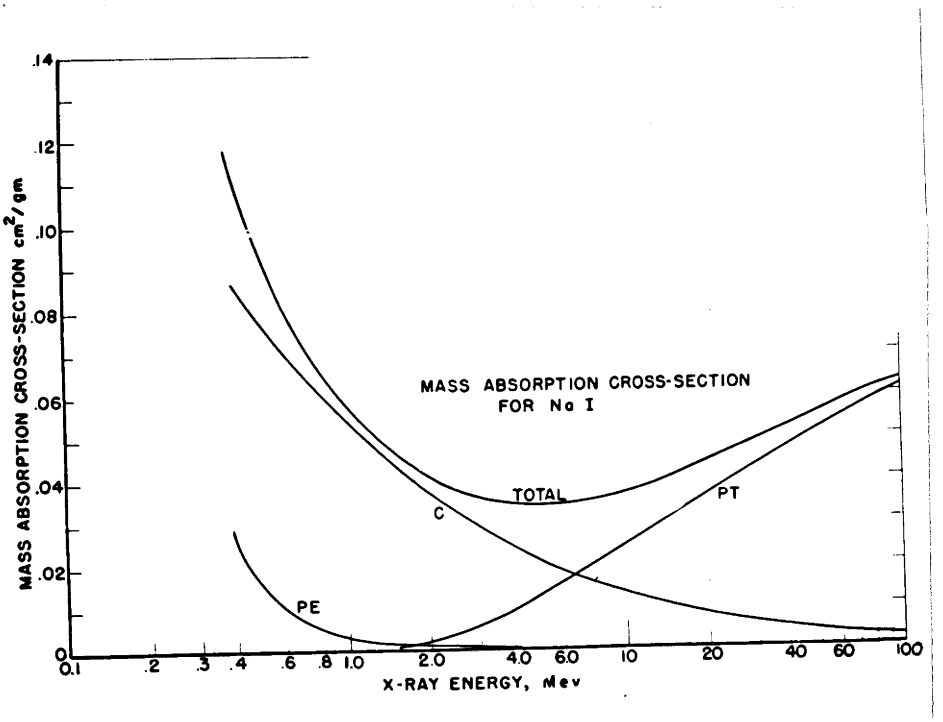


Fig. 2.5. Absorption processes in NaI in the region $E_\gamma$ = 0.1 to 100 Mev. The mass absorption cross section: Total = total pair production(PT) + Compton scattering (C) + photo-electric effect (PE) from Grodstein (Gr 57).

gamma rays in the $Li^7(p,\gamma)Be^8$ spectrum are obtained.

## 2.1. Absorption of Gamma Radiation in a Sodium Iodide Detector.

A gamma ray may be absorbed in the detector by three processes; electron pair formation, Compton scattering and the photoelectric effect. The cross section for each of these absorption processes varies with energy of the gamma ray as shown in figure 2.5. (Gr 57). At 17.6 Mev, the photoelectric effect is of no significance for the initial event in the absorption of a particular gamma ray, but is significant for low energy gamma rays which are the result of events in the absorption process. From the figure one can see at $E_\gamma$ = 17.6 Mev, that 79% of the initial interactions between the crystal and the gamma ray beam are pair creation events while the remainder are Compton scattering.

An analysis of the subsequent events which lead to the eventual total absorption of the initial gamma ray energy in the detector or to escape of some fraction of this energy, requires a calculation of the Monte Carlo type and has been performed for gamma ray energies up to 4.45 Mev for sodium iodide detectors of dimensions up to 8 in. radius by 8 in. long (Mi 58, Be 56). From these calculations an accurate prediction

can be made of the pulse height distribution of monochromatic gamma rays detected by a crystal of specified dimensions. For gamma rays of energy greater than 4 Mev the number of multiple events following an initial absorption event increases rapidly and the energy loss by the secondary electrons includes loss by bremsstrahlung which becomes more significant as the gamma ray energy increases. For these reasons the Monte Carlo calculations for the line shapes of high energy gamma rays become very elaborate even for the present generation of electronic computors.

## 2.2. Response of a NaI(Tl) Detector to Gamma Radiation.

Any investigation into the line shapes of high energy gamma rays must then involve the experimental approach. A synthesis of the pulse height distributions of 10 - 20 Mev monochromatic gamma rays for a 5 in. diameter by 9 in. long NaI(Tl) detector has been made by Koch and Wyckoff (Ko 56) by measuring the response of the crystal to monochromatic electrons from a betatron. Spectral lines for electron energies in 1 Mev intervals involved in pair formation from an incident gamma ray were folded together to predict the line shape due to the electron pairs. It has been assumed that the energy loss characteristics of electrons and positrons in the detector are the same, except for the production of annihilation radiation by positrons.

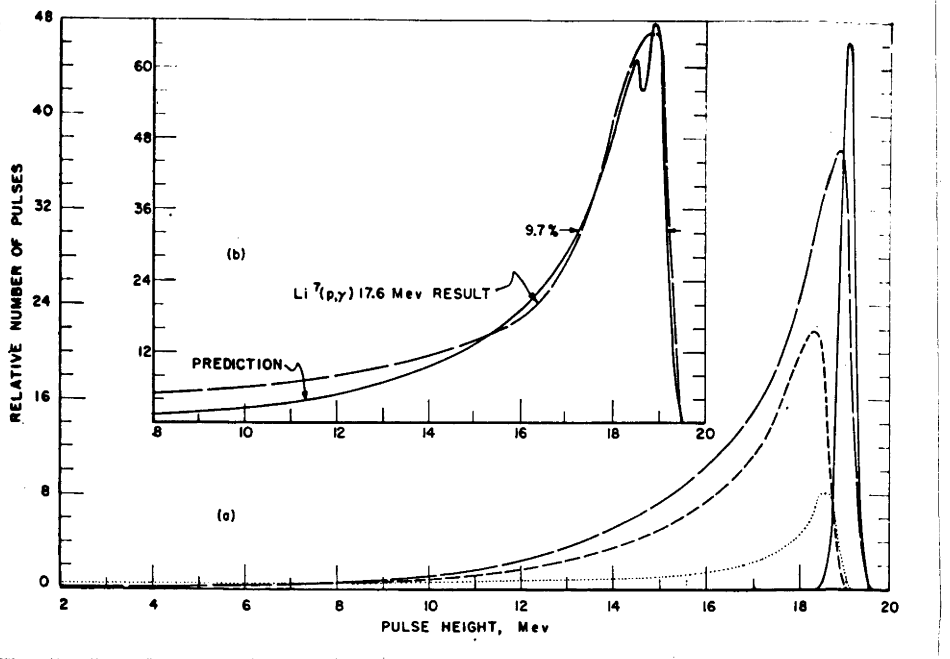


Fig. 2.6. Synthesis of the pulse height distribution of 19 Mev gamma rays in a 5 in. diameter by 9 in. long NaI crystal spectrometer. (after Koch and Wyckoff; (Ko 56)

1. Compton electron distribution(dotted curve)
2. Multiple Compton interactions that contribute to the photoline energy (solid curve).
3. Folded electron-pair distribution (long dashed curve)
4. Distribution due to loss of annihilation quanta (short dashed curve)

Insert. Composite distribution compared with experiment (Fo 54)

By extrapolation from the calculations of Berger and Doggett (Be 56) for gamma rays up to 4.5 Mev, they were able to estimate the electron distribution due to Compton scattering of photons, the fraction of totally absorbed gamma ray energy which gives rise to a gaussian distribution about the photo line, and the broadening of the pulse height distribution due to the escape of one of the annihilation photons from the detector. The latter process results in the downward displacement of a fraction of the electron pair pulse height distribution by 0.51 Mev.

Figure 2.6 shows their synthesis of the pulse height distribution of a 19 Mev gamma ray in a 5 in. diameter by 9 in. long NaI(Tl) detector. The four separate contributions to the line shape are shown and the prediction is compared with the 17.6 Mev gamma ray line shape from the $Li^7(p,\gamma)Be^8$ reaction. This was obtained by adjusting the 14.8 and 17.6 Mev gamma ray line shapes to fit the intensity ratio $I_{17.6}/I_{14.8} = 1.6$ (Fo 54).

An important conclusion from the synthesis is that the line shape of monochromatic gamma rays changes slowly from 10 to 20 Mev and this has been confirmed by direct measurement with 5 in. diameter by 4 in. and 8 in. long NaI(Tl) crystals (Ko 59).

The synthesis of Koch and Wyckoff has been

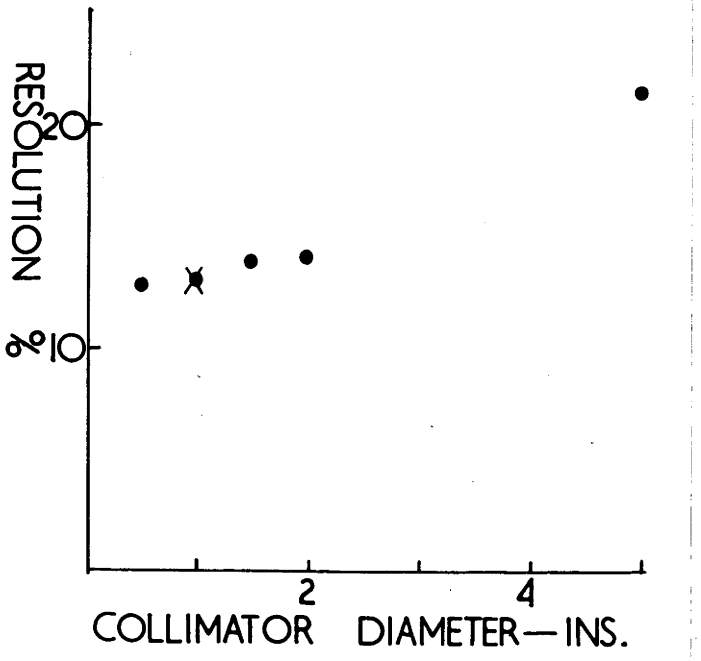


Fig. 2.7. Variation of resolution with collimator diameter for 20.4 Mev gamma ray. Point X has been measured with beam collimated along crystal axis. Points O by collimation through centre of crystal side.

made assuming fine collimation of the gamma ray beam along the crystal axis. For comparison with experiment, the effect of the collimator must be considered as well as scattering of the gamma ray beam by the target housing and the collimator wall.

2.3. Effect of Collimator Size.

By increasing the diameter of the collimated gamma ray beam, the probability of escape of radiation through the crystal sides increases and the pulse height distribution of the gamma ray broadens.

The pulse height distribution of 20.3 Mev gamma rays from proton capture in tritium was measured with the apparatus of figure 2.1 but using cylindrical collimators of varying diameter. The resolution was found to vary as shown in figure 2.7 and is relatively insensitive to collimator dimensions for those less than 1.5 in. diameter. One point is shown in figure 2.7 which has been obtained by collimating the beam along the crystal axis, and it was concluded that the optimum resolution of 13% could be attained with the crystal axis vertical. This orientation was found more convenient to use in the experiment.

2.4. Efficiency of the Detector.

From the total gamma ray absorption cross sections $\mu$ for NaI (Da 55) at $E_\gamma$ = 14.8 and 17.6 Mev,

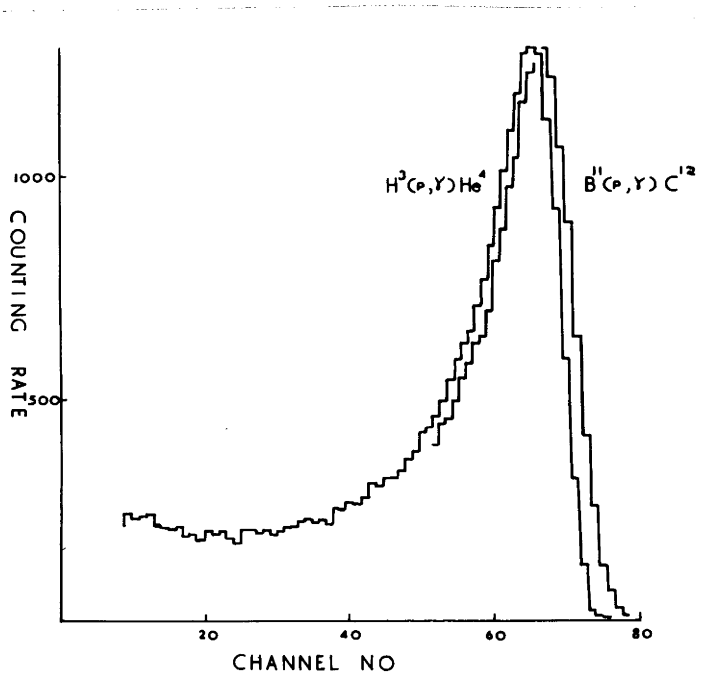


Fig. 2.8. Comparison of pulse height distributions of 16.6 and 20.4 Mev gamma rays from $B^{11}(p,\gamma)C^{12}$ and $H^3(p,\gamma)He^4$ respectively. For comparison, the $B^{11}$ $(p,\gamma)$ spectrum has been displaced to the right.

the efficiencies

$$E = 1 - e^{-\mu L} \qquad (L = 5 \text{ in.})$$

were found to be 82.8% and 84.5% respectively. No corrections were made for the 2 Mev width of the 14.8 Mev gamma ray.

2.5. The Line Shape of the 17.6 Mev Gamma Ray.

The 17.6 Mev gamma ray line shape is not directly available from the pulse height analysis of the $Li^7(p,\gamma)Be^8$ radiation because of the overlap of the two gamma rays in the spectrum (figure 2.3). The separation is complicated by the 2 Mev width of the 14.8 Mev component.

The 17.6 Mev line is monochromatic and it was decided to investigate the difference in the pulse height distributions of the 16.6 Mev and 20.4 Mev gamma rays from proton capture in $B^{11}$ and $H^3$ respectively to see if the 17.6 Mev line shape could be estimated from these two monochromatic gamma rays.

Thick targets of natural boron and tritium adsorbed on zirconium were placed in turn in the angular distribution chamber shown in figure 2.1 and were bombarded with 1 Mev protons. Because of the $\sin^2\theta$ angular distribution of the $H^3(p,\gamma)He^4$ reaction (Ar 50) the spectrometer was set at 90° with the target at 45° to the proton beam. The $B^{11}(p,\gamma)C^{12}$ reaction was observed

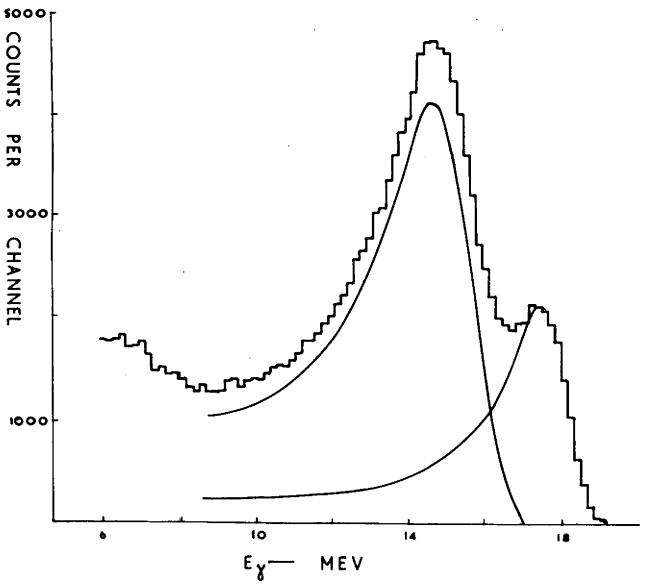


Fig. 2.9. Separation of the 14.8 and 17.6 Mev gamma rays from $Li^7(p,\gamma)Be^8$. ($E_p$ = 380 Kev, target 200 KeV thick, $\theta = 0°$).

at 0°. In addition, a 200 Kev thick lithium target was bombarded with 500 Kev and 380 Kev protons and the yield was observed at 0°. The gain and bias of the pulse height analyser were not altered during the comparison but the gain of the photomultiplier was altered by adjusting the E.H.T. supply so that the peak height of the 20.4, 17.6 and 16.6 Mev gamma rays occurred in turn in the same channel of the pulse height analyser. In figure 2.8, the 16.6 and 20.4 Mev gamma ray spectra, normalised to the same peak height, are compared. Because of the 12 Mev gamma ray from the $B^{11}(p,\gamma)C^{12}$ reaction, it was not possible to observe the 16.6 Mev line shape below 14 Mev. Above this energy there is no measurable difference in the two spectra and assuming the 17.6 Mev gamma ray has the same pulse height distribution, the separation of the two components in the $Li^7(p,\gamma)Be^8$ radiation is shown in figures 2.2 and 2.9.

## 2.6. The $Li^7(p,\gamma)Be^8$ Reaction at $E_p$ = 270 Kev.

One result of the present measurement of the angular distribution of the $Li^7(p,\gamma)Be^8$ radiation shows (Chapter IV) that at $E_p$ = 270 Kev, the 14.8 Mev gamma ray is isotropic while the 17.6 Mev component is anisotropic. Spectra observed at 0° and 135° at this energy after correction for the background, absorption

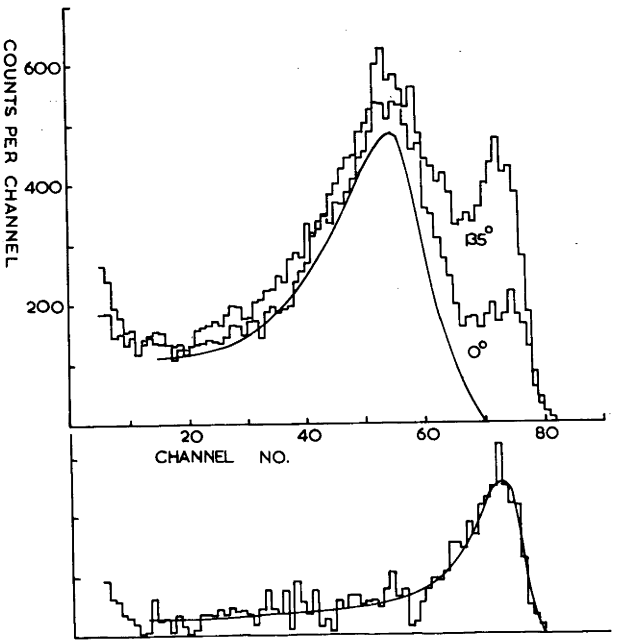


Fig. 2.10. $Li^7(p,\gamma)Be^8$ spectra at $E_p$ = 270 Kev, corrected and normalised to the same number of monitor counts. The lower curve shows the difference in the two distributions.

in the target backing and normalising the two observations to the same number of monitor counts are shown in figure 2.10. The subtraction of the two pulse height distributions is included in figure 2.10 and represents the line shape of the 17.6 Mev gamma ray. This curve was subtracted from the 0° spectrum to give the line shape of the 14.8 Mev component (figure 2.10). A smoother estimate of the 17.6 Mev component was obtained using a resonance spectrum obtained from the same target (figure 2.11). The 17.6 Mev line shape from figure 2.10 was normalised to the resonance spectrum and subtracted to obtain the approximate height of the 14.8 Mev component. The 14.8 Mev pulse height distribution was normalised to this height and subtracted from the resonance spectrum to give the 17.6 Mev line shape. The method is cumbersome and involves approximations but a comparison of the 17.6 line shape with the 20.4 Mev gamma ray justifies the assumption that the two pulse height distributions are similar.

## 2.7. Line Shape Below $E_\gamma$ = 8.5 Mev.

The pulse height distributions do not indicate the line shape below 8.5 Mev. In this energy region, contributions from the $F^{19}(p;\alpha,\gamma)O^{16}$ reactions are mixed with low energy gamma rays from scattered radiation. Many of these events arise from scattering material outside the detector and some are due to the escape from

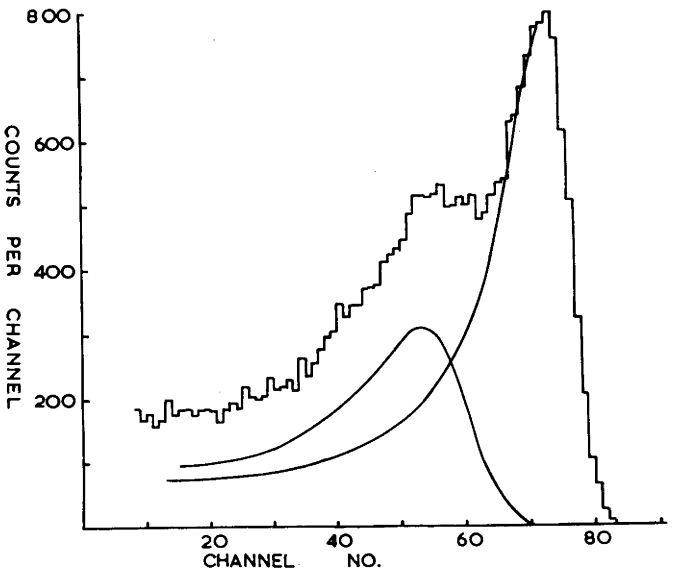


Fig. 2.11. Separation of the 17.6 and 14.8 Mev gamma rays from $Li^7(p,\gamma)Be^8$. ($E_p$ = 445 Kev, target 60 Kev thick).

the detector of a fraction of the incident gamma ray energy. The actual line shape between 0 and 8.5 Mev depends on the latter and is partly determined by the dimensions of the collimator. Calculations of the pulse height distribution of high energy gamma rays below $E_\gamma$ = 8 Mev show that with no collimation, the line shape maintains a constant height in this energy region (Ko 59). For the collimator used in these investigations, the line shape was assumed to be between the limits shown in figure 3.1. The angular distributions of the gamma rays were obtained without considering the spectra below $E_\gamma$ = 8.5 Mev and the line shape below this energy was only of interest in the calculation of the absolute value of the intensity ratio in Chapter III.

2.8. Conclusion.

The separation of figure 2.9 shows the 14.8 Mev gamma ray line shape does not extend beyond 16.9 Mev and the angular distribution of the 17.6 Mev component $W(\theta)_{17.6}$ can be obtained from the part of each spectrum above this energy. The angular distribution of the unresolved gamma rays $W(\theta)_{14.8 + 17.6}$ is calculated by summing each spectrum between 8.5 and 19.5 Mev. $W(\theta)_{14.8}$ can be derived from $W(\theta)_{14.8+17.6}$ and $W(\theta)_{17.6}$ after measuring the relative intensity of

the two components at $\theta = 90°$. For this reason, the variation of the ratio was measured from $E_p$ = 200 to 1030 Kev with a higher statistical accuracy than could be attained from the spectra in the angular distribution measurements.

# CHAPTER III.

## Measurement of the Branching Ratio.

Introduction.

In this work, the branching ratio is defined as the ratio of the intensity of the ground state transition to the intensity of the transition to the 2.9 Mev level of $Be^8$. The ratio is known to be a function of proton energy (Wa 48) but the only detailed measurement of the variation has been made using a 1-1/2 in. diameter by 1-1/2 in. long NaI(Tl) crystal (Ca 56). Because the gamma rays were not resolved, it was necessary to assume the line shape of each component and that the intensity ratio at the 441 Kev resonance was 1.7 (St 51).

A knowledge of the branching ratio for non-resonance radiation is of interest because the direct s wave proton capture mechanism of Wilkinson predicts the ratio to favour the transition to the first excited state of $Be^8$(Wi 54), for both jj and LS coupling schemes. It is not known if the ratio varies in the neighbourhood of the 1030 Kev resonance. Apart from these matters, the ratio is required to derive the angular distribution of the 14.8 Mev gamma ray $W(\theta)_{14.8}$ from $W(\theta)_{17.6}$ and $W(\theta)_{14.8 + 17.6}$.

2.1. Experimental.

The apparatus used in the measurement of the branching ratio has been described in Chapter II. The detector was set at 90° to the proton beam and currents of 10 - 15 μA were used except in the region of the 441

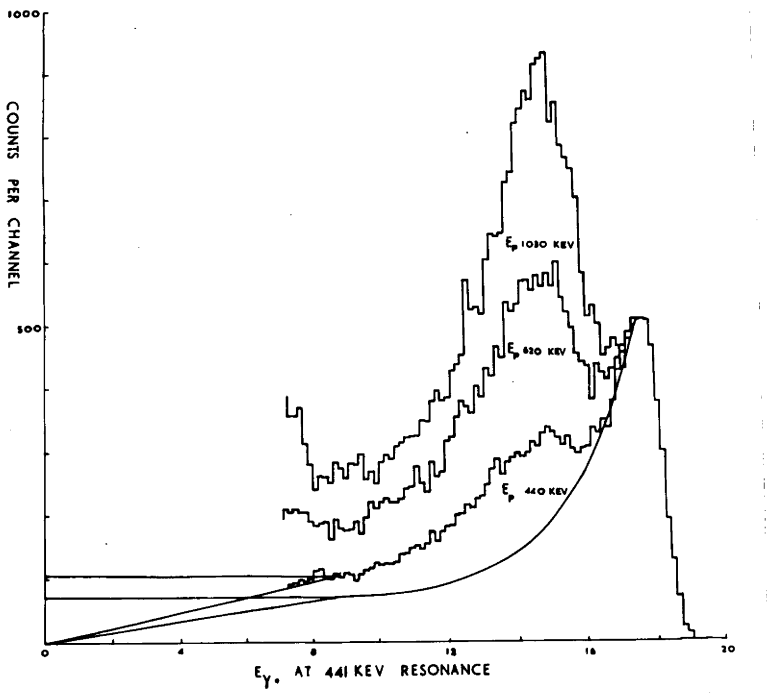


Fig. 3.1. Comparison of $Li^7(p,\gamma)Be^8$ spectra obtained at $\theta = 90°$ for $E_p$ = 440; 620 and 1030 Kev. The smooth curve is the line shape of the 17.6 Mev gamma ray.

Kev resonance where the beam intensity was reduced to avoid high counting rates. The targets were kept as thin as experimental conditions would allow. Between 430 and 450 Kev, the deposits were less than 5 Kev thick and between 450 and 600 Kev were 5 - 10 Kev thick. In the remaining energy regions, the targets were 20 Kev thick except for the points below $E_p$ = 300 Kev where the low yield required a 60 Kev target.

The bias and gain of the pulse height analyser were fixed during the measurements so that the peak height of the 17.6 Mev gamma ray fell in the same channel of the display. Measurements were made in 5 - 50 Kev intervals from $E_p$ = 200 to 1030 Kev. The running time and integrated beam current were noted for each observation and each spectrum was recorded from the display of the pulse height analyser. The cosmic ray background was measured by running the electronics for 1 to 2 hours with the accelerator switched off.

The pulse height distribution of the 17.6 Mev gamma ray was obtained by replacing the lithium target with a target of tritium adsorbed on zirconium. The target was bombarded with 850 Kev protons and the high voltage supply to the photomultiplier tube was reduced until the peak of the 20.3 Mev gamma ray coincided with the channel number of the 17.6 Mev gamma ray.

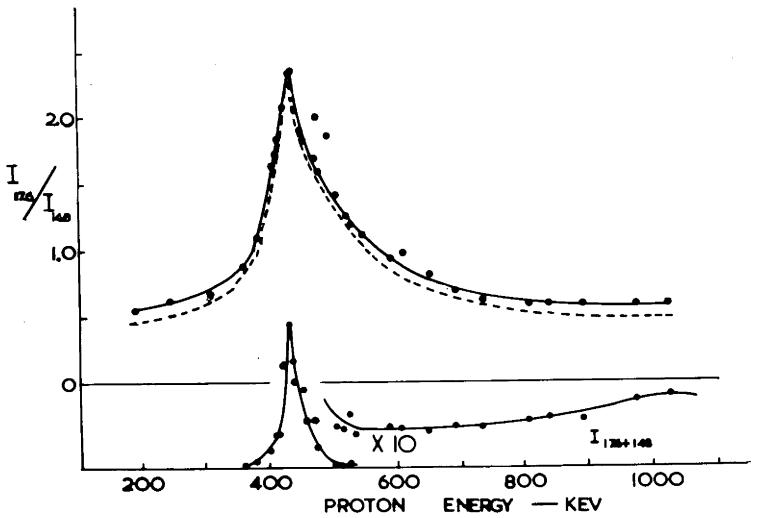


Fig. 3.2. Variation of the branching ratio with proton energy (upper curve) and the excitation function (lower curve).

Figure 3.1 shows typical spectra obtained in the measurement normalised to a common peak height at 17.6 Mev. The line shape of the gamma ray from $H^3(p,\gamma)He^4$ is included. The extrapolations to zero energy in figure 3.1 show the assumed limits in the line shape based on the calculations of Kockum and Starfelt (Ko 59).

2.2. Calculation of the Branching Ratio.

Each spectrum was summed between $E_\gamma$ = 8.5 and 19.5 Mev and the cosmic ray background was subtracted. The assumed pulse height distribution of the 17.6 Mev component was normalised to fit each spectrum and the intensity of the 14.8 Mev component was obtained by subtraction.

The variation of the ratio with proton energy is shown in the upper curve of figure 3.2. The excitation function in the figure was derived from the ratio of the number of counts between $E_\gamma$ = 8.5 Mev and 19.5 Mev and the number of monitor counts. Four targets of varying thickness were used in the investigation and the yields at the 441 Kev resonance were normalised to a common value. The smooth curve above $E_p$ = 800 is that measured by Kraus (Kr 54) at $\theta = 90°$.

2.3. Absolute Value of the Branching Ratio.

The results of figure 3.2 are those required

in the separation of the angular distributions but further corrections are necessary to estimate the absolute value of the ratio.

The errors in the absolute value due to the uncertainty in the line shape below $E_\gamma$ = 8.5 Mev have been calculated assuming the extrapolations of figure 3.1. At the 441 Kev resonance, the ratios are within 3% of the value shown in figure 3.2 while at $E_p$ = 770 Kev, the ratios are 0.50 ± 0.01 and 0.54 ± 0.01 for the upper and lower limits, compared with 0.58 ± 0.01 in figure 3.2. The broken curve in figure 3.2 shows the lower limit in the absolute value of the ratio due to the uncertainty in the line shape. A small correction was made for the variation of the detector efficiency (Chapter II, 2.4). The upper limit in the absolute value of the ratio approximates to the experimental curve.

3. Discussion.

The points at $E_p$ = 480 and 500 Kev show higher values of the ratio than neighbouring points and this effect is attributed to non-uniformity of the target deposit where a small portion may be thick enough to contribute some resonance radiation with a larger cross section and a higher value of the ratio. In this case,

TABLE 3.1.

Measurements of the $Li^7(p,\gamma)Be^8$ branching ratio.

| $E_p$ (Kev) | Target Thickness (Kev) | Angle | $b = \frac{I\ 17.6}{I\ 14.8}$ | Reference. |
|---|---|---|---|---|
| 450 | 10-20 Kev | 0°,90° | $2 \pm 0.2$ | (De 50) |
| 460 | 150 Kev | 0° | 2 | (Wa 48) |
| 500 | Thick | 0°<br>35°<br>70° | $1.7 \pm 0.2$<br>1.8<br>1.72 | (St 51) |
| 1150 | 70 | 0°? | .66 | (Wa 48) |
| 1150 | 250 | 0°<br>35°<br>75° | $.62 \pm 0.07$<br>.58<br>$.45 \pm 0.1$ | (St 51) |
| 200 | Thick | 90° | $.5 \pm 0.1$ | (Ca 56) |
| 375,600 | Thin | 90° | $1.0 \pm 0.2$ | (Ca 56) |

the target was discarded and the measurement was repeated.

The precautions taken to minimise this effect have been described in Chapter II but there remains a possibility that the measured value of the ratio in the region of 460 - 650 Kev may be too high. Nevertheless, the points on the curve are repeatable; and the asymmetry in the branching ratio about $E_p$ = 441 Kev has been observed by other investigators (De 49, Ca 56).

The ratio at the 441 Kev resonance is 2.3 ± 0.04 and higher than measurements reported by other workers (Table 3.1). In those investigations, thick targets were used and the inclusion of a small amount of non-resonant radiation would tend to reduce the relative intensity of the 17.6 Mev gamma ray. It is interesting to refer to the resonance spectrum of figure 2.2 obtained from a 200 Kev thick target, bombarded with 500 Kev protons. The intensity ratio obtained from this spectrum was 1.80 ± 0.02.

In the region of the 1030 Kev resonance, the intensity ratio maintained a constant value at 0.58 ± 0.01 (uncorrected) and both gamma rays are resonant.

About $E_p$ = 700 Kev, the radiation is largely due to the non-resonant background and the intensity ratio, 0.54 ± 0.05, is approximately independent of the angle of observation (Chapter IV). Integration of the ratio over

$4\pi$ does not alter the value and it is consistent with Wilkinson's prediction from the direct s wave proton capture mechanism that the transitions should favour the 2.9 Mev level of $Be^8$ (Wi 54).

In the neighbourhood of the 441 Kev and 1030 Kev resonances, the ratio was found to be a strong function of the angle of observation and this matter is investigated in the chapter which follows.

# CHAPTER IV.

## The Angular Distributions.

1. Introduction.

Theoretical expressions for the differential cross section of a nuclear reaction are given in the form:

$$d\sigma = \sum_{k=0}^{k_{max.}} B_k P_k \cos\theta. \quad \text{(Bl 52, De 57, Vo 59)}$$

where $\theta$ is the angle between the incident and emergent particles in the centre of mass system. For radiative capture processes, the system before collision can be defined in terms of the mutual orbital angular momentum l of the target nucleus and the bombarding particle and the vector sum s (channel spin) of their intrinsic angular momenta I and i respectively. The outgoing channel for gamma ray emission is expressed in terms of the multipole order of the gamma ray l' and the spin of the final nuclear state I'. Expressions in this representation show $B_k$ to be functions of the energy of the incident particle, the channel spins, the orbital angular momenta and the nature of the forces between the particles (De 57, Go 59).

Experimentally, the essential part of the analysis of angular distribution measurements is the expression of the observations in the centre of mass system and the calculation by the method of least squares

of the coefficients $B_k$ of the Legendre polynomials. There are a number of restrictions limiting the order k of the polynomials (Ya 48, Bl 52) which are important in the analysis and interpretation of angular distributions:

1. As a result of the conservation of parity, $B_k$ vanishes for odd values of k, provided the reaction involves an isolated level of the compound nucleus with unique parity and angular momentum. Odd powers of cos $\theta$ in an angular distribution are due to interference between odd and even parity interactions.

2. In reactions where the penetration coefficients are such that there is a maximum value l or l' for which the widths are significant, $k \leq 2l$; $k \leq 2l'$ and $k = 2b$ where b is the total angular momentum of the system.

In addition, there are a number of well-known selection rules concerning the emission of gamma radiation which are pertinent to the analysis of the angular distributions and which are included for completeness:

1. In a radiative transition between initial and final states of angular momenta J and I respectively, l can assume any non-zero integral value given by

$$|J - I| \leq l \leq |J + I|$$

2. The probability of emission of a gamma ray

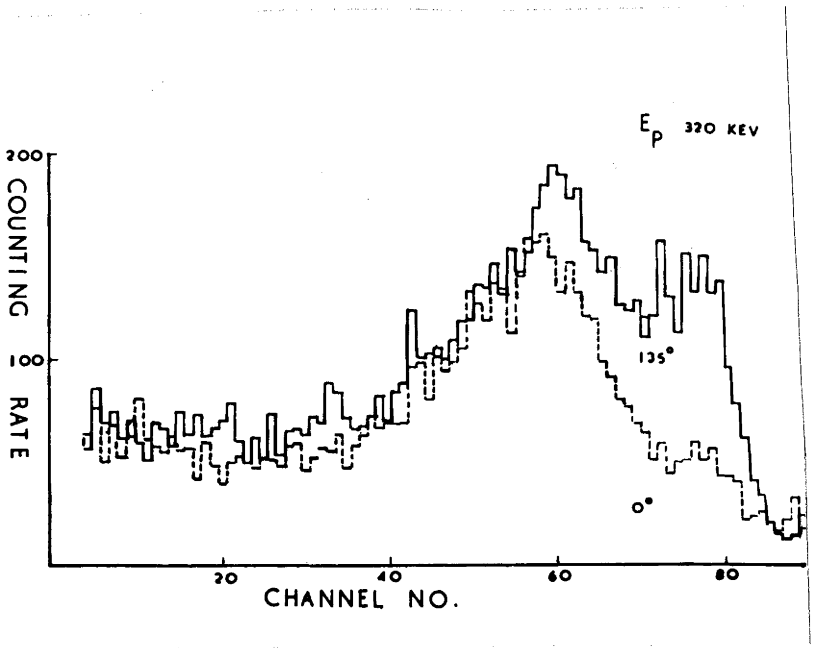


Fig.4.1. $Li^7(p,\gamma)Be^8$ spectra.

($E_p$= 320Kev; $\theta$ = 0° and 135°; target 20Kev thick).

in a transition J $\longrightarrow$ I decreases rapidly as l increases, roughly as $(\frac{2R}{\lambda})^{2l}$ (We 51, Bl 52a) where R is the nuclear radius and $\lambda$ is the wavelength of the emitted radiation. The multipolarity of the emitted radiation will generally correspond to the smallest value of l which is allowed by conservation of angular momentum and parity.

3. The relative transition probability of electric radiation is greater than magnetic radiation of the same multipolarity by a factor which is approximately

$$1/10\ (2\pi\ McR/h)^2$$

(We 51) where M is the mass of the nucleon. This approximates to $4.4A^{2/3}$ and for $Be^8$, the factor is of the order of 18, irrespective of the transition energy.

The facts summarised in this introduction are used in the analysis of the angular distributions in section 3.1 and a summary of the results is included in the final sections. First, the measurement of the distributions is described.

2. Experimental.

Measurements of the energy spectra were made at 8 to 10 angles of observation, chosen in random order but at approximately equally spaced intervals of cos $\theta$ between 1 and - 0.71. The targets were set in a plane perpendicular to the proton beam but for measurements

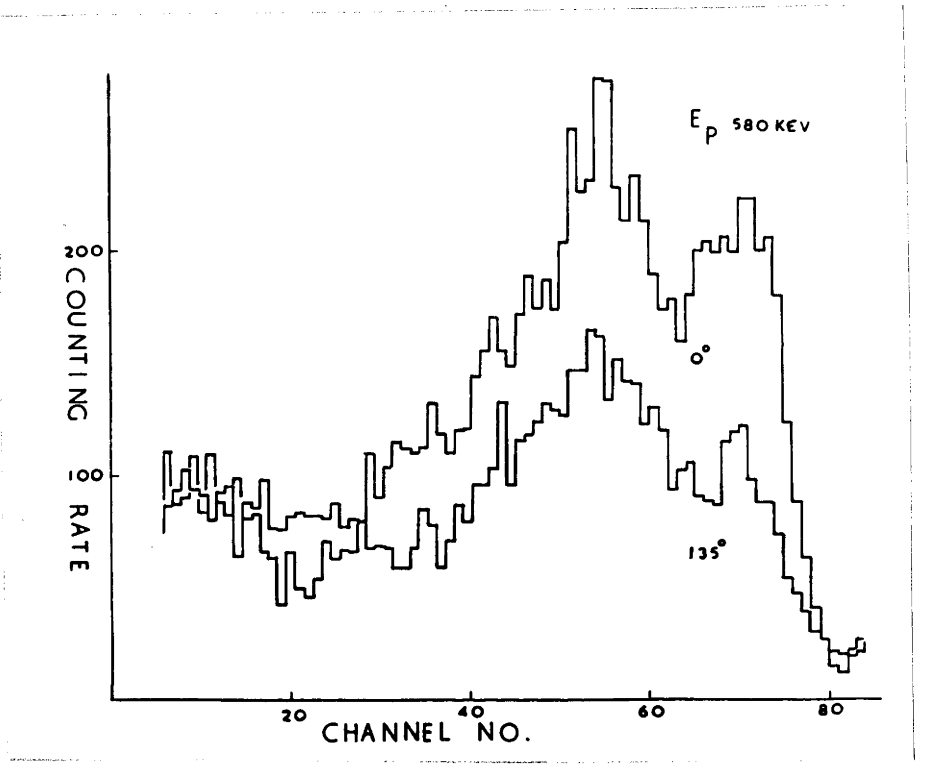


Fig. 4.2. $Li^7(p,\gamma)Be^8$ spectra.

($E_p$=580Kev; $\theta$ = 0° and 135°; target 10Kev thick).

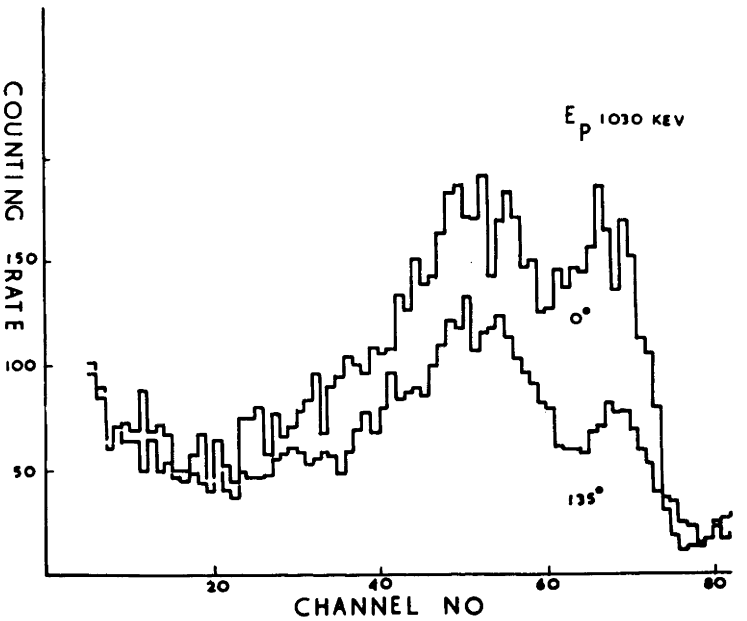


Fig. 4.3. $Li^7(p,\gamma)Be^8$ spectra.

($E_p$ = 1030Kev; $\theta$ = 0° and 135°; target 10Kev thick).

at 90°, the backing was inclined at an angle of 20° to the beam. Rotation of the target was not considered desirable because the resulting increase in target thickness effectively reduces the beam energy. A rotation of the target through 20° increases the thickness by 6% and this variation was considered tolerable even in the regions where the angular distributions change rapidly with proton energy. Earlier workers showed $W(\theta)_{14.8 + 17.6}$ varied rapidly between 400 and 550 Kev (De 49) and between 950 and 1100 Kev (Kr 54). In these energy regions, targets 10 Kev thick were found to effect the compromise between the need for a thin target and an adequate yield from the reaction. At the 441 Kev resonance, targets less than 5 Kev thick were used and in the remaining energy regions, 20 Kev thick targets were used except for points below $E_p$ = 300 Kev where the low yield required targets 40 Kev thick. Figures 4.1 to 4.4 show typical spectra obtained in the measurements.

The angular distributions of the unresolved gamma rays were calculated from the sum of events between $E_\gamma$ = 8.5 and 19.5 Mev, and the spectra were summed between the channels corresponding to 16.9 and 19.5 Mev to derive the angular distribution of the 17.6 Mev component. The totals, after correction for cosmic ray background, absorption in the target backing, counting

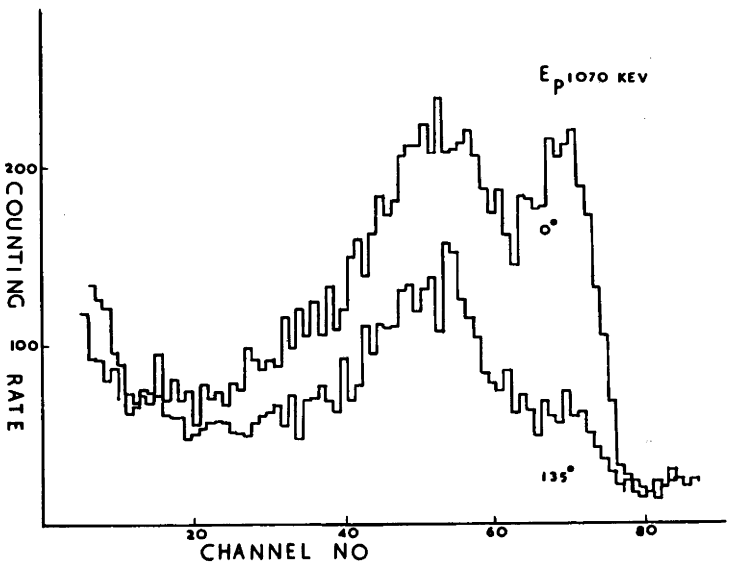


Fig. 4.4. $Li^7(p,\gamma)Be^8$ spectra.

($E_p$=1070Kev; $\theta$ = 0° and 135°; target 10Kev thick).

loss in the pulse height analyser and normalisation to the same number of monitor counts, were expressed with the angle of observation in the centre of mass system.

In the corrections, the following approximations were made:

1. The absorption coefficients for brass at $E_\gamma$ = 14.8 and 17.6 Mev (0.032 and 0.034 $cm^2/gm$ respectively (Da 55)) were assumed to be 0.033 $cm^2/gm$ and constant over the $(E_\gamma + 7/8E_p)$ Mev range investigated. The use of this average value gave rise to a maximum error of 0.02% in the correction factor for absorption.

2. The transformation of the intensity $I(\theta)$ and angle of observation, $\theta$ in the laboratory system to the centre of mass system,

$$I(\theta)_{c.m.} = I(\theta) \frac{(1 - v^2/c^2)}{(1+v/c \cos \theta_{c.m.})^2}$$

and $$\cos \theta_{c.m.} = \frac{\cos \theta - v/c}{1 - v/c \cos \theta}$$

approximate to

$$I(\theta)_{c.m.} = I(\theta) \cdot (1 - 2v/c \cos \theta)$$

and $$\theta_{c.m.} = \theta - 2 v/c \sin \theta$$

if higher powers than the first in v/c are neglected, v being the velocity of recoil of $Be^8$. The highest value of v/c in this investigation is 0.006 at $E_p$ = 1100 Kev.

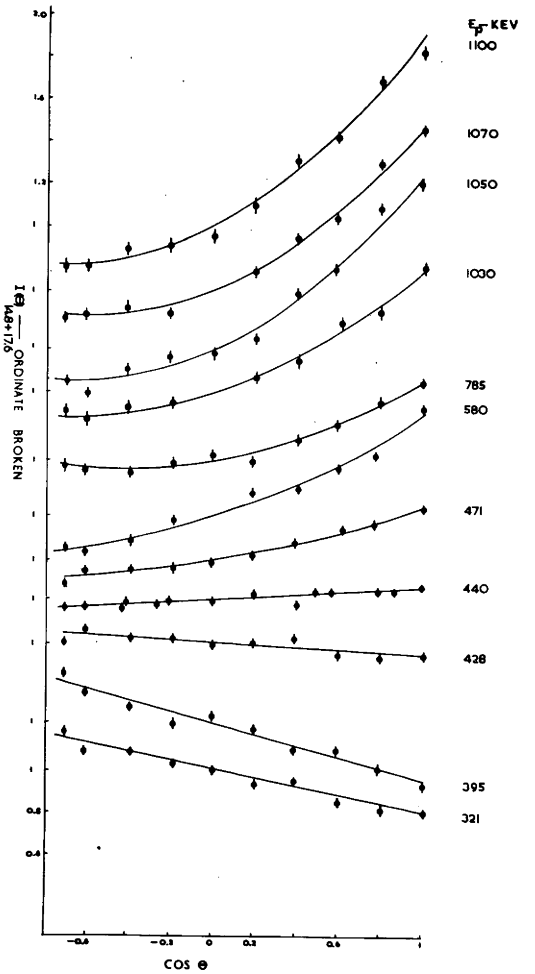


Fig. 4.5 Angular distributions of the unresolved gamma rays $W(\theta)_{14.8+17.6}$

Experimental points for $W(\theta)_{14.8 + 17.6}$ and $W(\theta)_{17.6}$, normalised to unity at cos $\theta$ = 1 are shown in figures 4.5 and 4.6.

3.1. Analysis.

It can be seen from figures 4.5 and 4.6 that the angular distributions are not symmetrical about $\theta = \pi/2$ ; and odd powers of cos $\theta$ are present indicating interference between contributions from protons of odd and even parity. Assuming the current evidence that both resonances are due to odd parity (p wave) protons (Chapter I, 1.3), the interfering radiation must be due to even parity protons. In this proton energy range, the penetrability of l = 2 protons is of the order of 0.2% of that for l = 0 protons (Ch 48) and the interference is assumed to be predominantly s - wave with a small admixture of d- wave protons.

The ground state of $Li^7$ is $3/2^-$ and electric dipole (El) radiation can rise from both s and d wave proton capture in this nucleus. Since El radiative transitions are more probable than magnetic on higher order electric radiation, the interference is assumed to be El. For s - wave proton capture, the radiation would be isotropic and for d wave protons, the highest order term in the angular distribution function would be $\cos^2\theta$. Interference between radiation from d wave

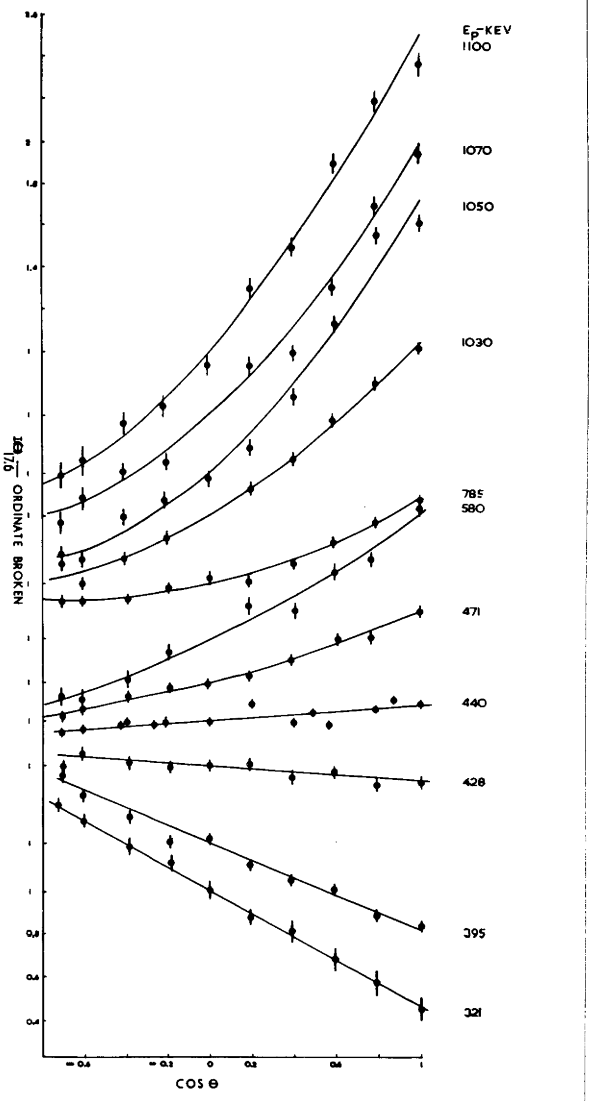


Fig. 4.6 Angular distributions of the 17.6 Mev gamma rays $W(\theta)_{17.6}$

TABLE 4.1.

Values of the coefficients of the angular distributions in figures 4.1 and 4.2.

| Proton Energy (Kev). | 14.8 + 17.6 Mev. | | 17.6 Mev. | | 14.8 Mev. | |
|---|---|---|---|---|---|---|
| | $A_1/A_o$ | $A_2/A_o$ | $A_1/A_o$ | $A_2/A_o$ | $A_1/A_o$ | $A_2/A_o$ |
| 1100 | 0.52 | 0.35 | 1.15 | 0.4 | 0.16 | 0.32 |
| 1070 | 0.41 | 0.36 | 0.90 | 0.39 | 0.14 | 0.34 |
| 1050 | 0.46 | 0.36 | 0.87 | 0.43 | 0.23 | 0.32 |
| 1030 | 0.31 | 0.26 | 0.56 | 0.23 | 0.17 | 0.28 |
| 786 | 0.18 | 0.2 | 0.20 | 0.17 | 0.15 | 0.22 |
| 581 | 0.33 | 0.14 | 0.49 | 0.10 | 0.17 | 0.18 |
| 471 | 0.17 | 0.08 | 0.20 | 0.07 | 0.12 | 0.10 |
| 440 | 0.056 | 0.008 | 0.064 | 0.015 | 0.036 | -0.002 |
| 428 | -0.057 | -0.029 | -0.070 | 0.004 | -0.032 | -0.095 |
| 396 | -0.27 | -0.02 | -0.41 | 0.04 | -0.09 | -0.09 |
| 321 | -0.22 | 0.01 | -0.56 | 0.00 | -0.01 | 0.02 |

interaction and the E2 component in the resonant 14.8 Mev gamma ray would introduce a $\cos^3\theta$ term in $W(\theta)_{14.8}$ (Br 60).

The angular distributions would then be of the form:

$$W(\theta)_{14.8} = A_o + A_1 \cos\theta + A_2 \cos^2\theta + A_3 \cos^3\theta \quad --(5)$$

and $$W(\theta)_{17.6} = A_o + A_1 \cos\theta + A_2 \cos^2\theta \quad ----(6)$$

A number of the measurements of $W(\theta)_{14.8+17.6}$ were analysed in the form of equation (5) but the errors in $A_3$ were large and no significance could be attributed to the values.

The solid lines in figures 4.5 and 4.6 show the results of a least squares fit of the polynomials (6) to the experimental points. Errors in $A_1$ and $A_2$ have been estimated from statistical and possible geometrical errors in the measurement. Corrections of the coefficients for finite detector geometry were negligible (Ro 53, Go 59).

The angular distributions of the 14.8 Mev gamma ray, $W(\theta)_{14.8}$ were obtained analytically from the measurements. $W(\theta)_{17.6}$ was multiplied by the factor required to satisfy the condition that at $\theta = \pi/2$

$$\frac{W(\theta)_{17.6}}{W(\theta)_{14.8 + 17.6} - W(\theta)_{17.6}} = b \quad , \text{ the branching}$$

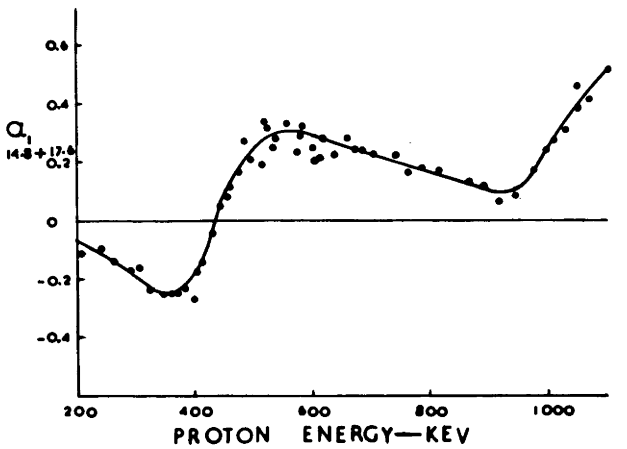


Fig. 4.7. Variation of $a_1$ in $W(\theta)_{14.8 + 17.6}$.

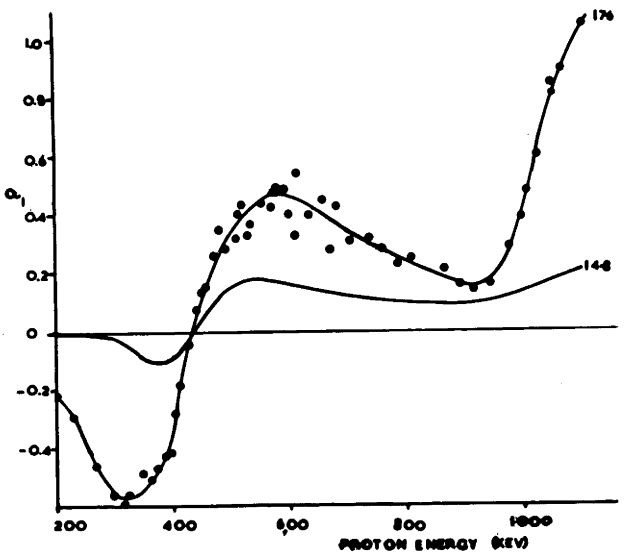


Fig. 4.8. Variation of $a_1$ in $W(\theta)_{17.6}$ and $W(\theta)_{14.8}$.

ratio measured at $\theta = \pi/2$ (Chapter III) and $W(\theta)_{17.6}$ was then subtracted from $W(\theta)_{14.8 + 17.6}$.

The angular distributions were expressed in the form $A_o (1 + a_1 \cos \theta + a_2 \cos^2 \theta)$. The coefficients of $W(\theta)$ for figures 4.5 and 4.6 are summarised in table 4.1 and the derived coefficients of $W(\theta)_{14.8}$ are included.

Figures 4.7 to 4.10 show the variation with proton energy of $a_1$ and $a_2$ for the resolved and unresolved gamma rays. The coefficients for $W(\theta)_{14.8}$ have been derived from the smoothed values of $W(\theta)_{14.8 + 17.6}$ and $W(\theta)_{17.6}$ but the variation of $a_2$ for the 14.8 Mev gamma ray is not shown because it is identical with $a_2$ in figure 4.9. This figure also includes measurements of $a_2$ by other workers (De 49, Kr 54). The excitation function of figure 4.9 is taken from figure 3.2 and above $E_p$ = 800 Kev the more accurate measurement by Kraus at $\theta = \pi/2$ (Kr 54) has been used.

In figures 4.7 and 4.8, the scatter of the values of $a_1$ between $E_p$ = 500 and 600 Kev is wider than experimental errors would allow. Energy straggle in the target can be serious in this energy region because of the rising cross section of the adjacent resonance and the rapid change in $a_1$. A comparison of the large number of spectra obtained in this energy region failed to reveal any significant difference in the relative intensity of the 17.6 Mev gamma ray at a particular

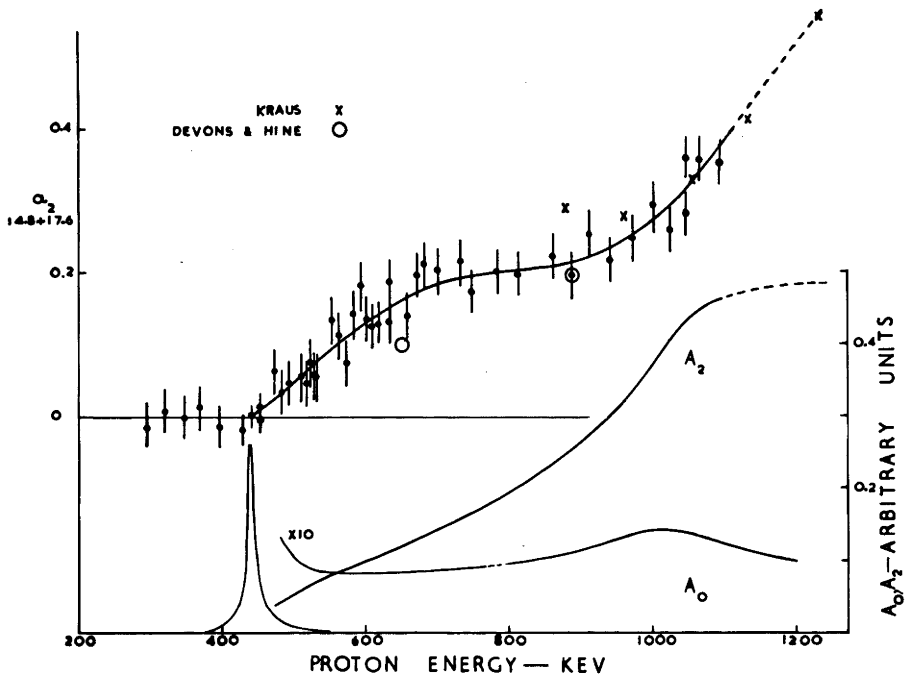


Fig. 4.9. Variation of $a_2$ in $W(\theta)_{14.8+17.6}$.

angle of observation. Nevertheless, the values of $a_1$, because of the energy straggle in this region, may be lower than one would expect from an ideally thin target.

3.2. The Variation of $a_2$.

An inspection of figures 4.9 and 4.10 shows the values of $a_2$ to be the same for both gamma rays within the experimental errors. The appearance of $a_2$ immediately above the 441 Kev resonance suggests that it is associated with the non-resonant background.

At the 441 Kev resonance $a_2$ is approximately zero, and neglecting interference effects, the radiation is isotropic.

At the 1030 Kev resonance, the situation is not immediately clear. If each value of $a_2$ is multiplied by the value at the corresponding point on the excitation function, the resulting $A_2$ is seen to rise steadily through the resonance (figure 4.9). Measurements of $A_2$ up to $E_p$ = 1240 Kev by Kraus (Kr 54) suggest that $A_2$ continues to rise slowly beyond the resonance and the finite value of $A_2$ can be attributed to the non-resonant background. If this is correct, the resonant radiation is isotropic.

3.3. The Variation of $a_1$.

Interference terms in $W(\theta)_{14.8 + 17.6}$ have been observed by earlier workers (De 49, Kr 54) but

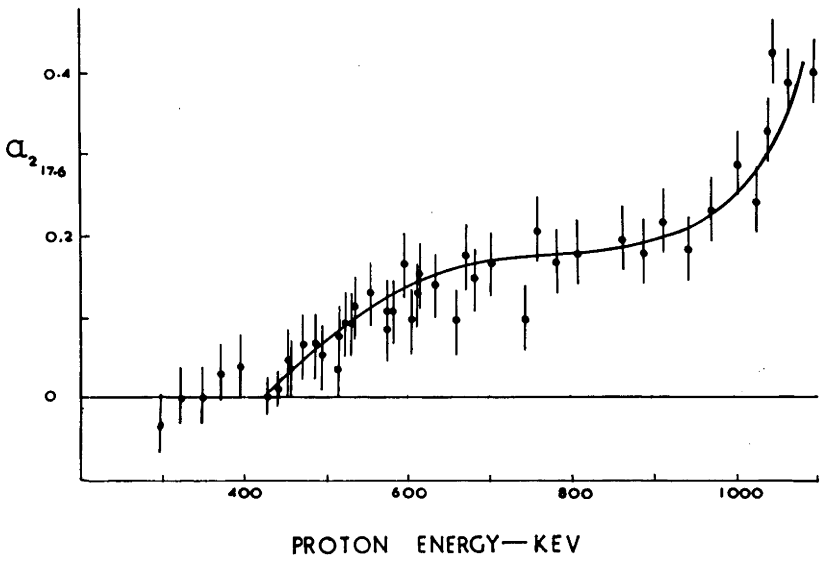


Fig. 4.10. Variation of $a_2$ in $W(\theta)_{17.6}$

the separation of the two gamma rays shows the interference to be stronger for the ground state transition than for the transition to the 2.9 Mev level of $Be^8$ and this effect appears to account for the difference in the angular distribution of the two components.

The magnitude of the interference for each gamma ray would depend on the relative intensity of the component at the resonance and in the interfering background. For the 14.8 Mev gamma ray, the interference would also depend on the undertermined mixing ratio of M1 + E2 at the resonance.

## APPENDIX.

## Calculation of the Coefficients of the Polynomials W(θ) by the Method of Least Squares.

This was performed using standard routines K3 and L7 of the computor Silliac in the Basser Computing Laboratory at the University of Sydney.

Routine K3 fits a set of N weighted † experimental points to the best polynomial of the form:

$$F(x) = \frac{1}{2} \sum_{s=0}^{s=n-1} a_s x^s \qquad (n - N)$$

The criterion of excellence for the polynomial is that the sum of the squares of the deviations,

$$M = \sum_{i=0}^{M-1} \left[ F(x_i) - f(x_i) \right]^2 . \; a_w(x_i)$$

where the $f(x_i)$ are the given experimental data, shall be a minimum with respect to arbitrary variations of the coefficients $a_s$.

The condition that M is a minimum is equivalent to a set of n simultaneous linear equations for the coefficients $a_s$. The programme produces the equations in a nx(n+1) matrix form which are used in the automatic solution of linear equations by routine L7.

---

† In the programme used, the experimental points were given equal weight.

# CHAPTER V.

Introduction.

This chapter extends the discussion of the experimental results and includes a comparison with the results of other workers. It is convenient to discuss separately the resonances, the non-resonant background and the observed interference between the two. The chapter ends with summary of the conclusions from the experiment and a brief discussion of further investigations which are suggested by the experimental results.

1. The 441 and 1030 Kev Resonances.

In this section the resonances are discussed ignoring the cos θ term in the angular distributions which is due to the interference of radiation of opposite parity to the resonance radiation.

1.1. The 441 Kev Resonance.

The approximate isotropy of the radiation from the 441 Kev resonance first led to the conclusion that the 17.64 Mev level of $Be^8$ was formed by s wave (l=o) protons (De 49). This was reconsidered (De 50, De 54) in the light of the analysis of the elastic scattering of protons by $Li^7$ at this resonance. (Co 49, Ch 53) which attributed the resonance to p wave protons. Capture of l = 1 protons by $Li^7(J=3/2^-)$ to the $J = 1^+$ level of $Be^8$ can proceed through channel spins 1 and 2; the contributions of both channels

overlap incoherently and cannot interfere with each other. The angular distribution of the resonance radiation is of the form (De 50)

$$W(\theta)_{17.6} = 1 + \cos^2\theta \frac{(5R-1)}{(5R+7)} \qquad \text{----(5.1)}$$

and

$$W(\theta)_{14.8} = 1 + \cos^2\theta \frac{(5R-1)(4+45\beta \sin \phi + 9\beta^2)}{260R+268 + 12\beta \sin \phi(1-5R)+3\beta^2(35R+41)} \qquad \text{-----(5.2)}$$

where R is the ratio of the contribution from channel spin 1 to channel spin 2, $\beta$ is the mixing ratio of E2 and M1 radiation and $\phi$ is the phase difference of the M1 and E2 multipoles.

For $R = {}^1/_5$, the angular distributions of the 17.6 and 14.8 Mev components are isotropic, irrespective of the relative strengths of M1 and E2 radiation in the 14.8 Mev gamma ray.

The angular distributions of the radiation at the 441 Kev resonance are, by the present measurements:

$$W(\theta)_{17.6} = 1 + .064 \pm .01 \cos\theta + 0.015 \pm .02 \cos^2\theta$$

$$W(\theta)_{14.8} = 1 + 0.036 \pm .02 \cos\theta - 0.002 \pm .03 \cos^2\theta.$$

The values of $a_2$ are approximately zero and consistent with a channel spin ratio of ${}^1/_5$.

Neuert and Retz-Schmidt (Ne 58) have observed a small $\cos^2\theta$ term ($a_2 = 0.03$) in the angular distributions of the two components corresponding to a channel spin ratio of ${}^1/_4$. The scatter of points in the

forward direction throws doubt on their conclusion although the value is within the experimental error of the present work. Devons and Hine (De 49) found $a_2 = o$ at this resonance for the unresolved gamma rays.

12. The 1030 Kev Resonance.

At the 1030 Kev resonance, it is difficult to measure the angular distribution of the resonance radiation in the presence of the non-resonant background which is dominant and certainly includes an $a_2$ term. If one assumes that the non-resonant background has a value of $a_2 = 0.24$ at $E_p = 1030$ Kev, it is only possible to say that within the experimental errors, the angular distribution of the resonant 17.6 Mev gamma ray is between $1 + .33 \cos^2\theta$ and $1 - 0.06 \cos^2\theta$. Since the resonance is believed to be p - wave (Li 55) equations 5.1. and 5.2. are again applicable and the channel spin ratio is between R = 0.1 and 1.

For a value of R other than $1/5$, $a_2$ is not necessarily the same for the two gamma rays (Eq.5.2) but since $\beta$ and $\phi$ are not known, no use can be made of these values to limit the errors in the ratio. The experimental results are not conclusive but the $Li^7(p,p)$ measurements at this resonance require a channel spin ratio of about $1/5$ (Li 55) and the present measurements of the gamma radiation are not inconsistent with this ratio.

2. The Non-Resonant Background.

The background radiation above the 441 Kev resonance was observed by Bonner and Evans who showed that it could not be explained in terms of the increased barrier penetrability of the resonant protons (Bo 48). No neighbouring resonances have been found that are strong enough to account for the cross section of the reaction between the resonances.

Wilkinson's theory of direct s-wave proton capture (Wi 54) is attractive because it can account for the background up to $E_p$ = 1 Mev, it predicts that in the non-resonant regions, the 2.9 Mev level of $Be^8$ is favoured in the capture process and the radiation (E1) has the correct parity to interfere with the 441 and 1030 Kev resonances. The theory would also require the background radiation to be isotropic but this is not in agreement with the experimental results. In the energy region investigated, s-wave proton capture is dominant but small contributions from l = 1 or l = 2 protons, while not contributing significantly to the total cross section could introduce a $\cos^2\theta$ term in the angular distributions. The penetrability of l = 2 and l = 1 protons is low in this region but large $a_2$ terms can arise from s-wave and d-wave interference in the background while s-wave and p-wave interference would introduce terms in cos θ only. In figures 4.9

and 4.10, $a_2$ terms appear at about $E_p$ = 460 Kev and this corresponds to the energy where the d-wave proton penetrability curve for $Li^7$ begins to rise (Ch 48). It is concluded that the non-resonant background includes both s and d-wave proton capture radiation which is assumed to be electric dipole in character. Contributions from l = 1 protons in the background may be present but would be limited by the longer mean life time of M1 and E2 radiation,

The $a_2$ term is then essentially an interference term from s and d- wave protons in the background; the variation of $a_2$ depends on the relative strength of the two components. According to Wilkinson, the direct s-wave proton capture cross section drops slowly beyond $E_p$ = 1 Mev and one would expect $a_2$ to show this effect. This has not been investigated quantitatively but the plateau in $A_2$ in figure 4.9, which lies beyond the present measurements, may be due to the change in the relative intensity of the s and d-wave proton contributions.

3. Interference.

Interference in the neighbourhood of the 441 Kev resonance was first observed by Devons and Hine (De 49) by measuring the intensity of the unresolved

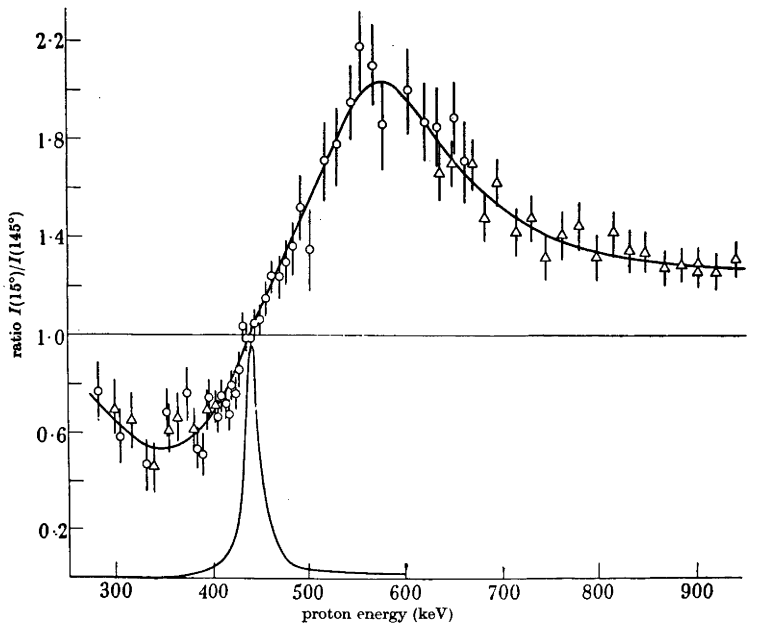


FIGURE 4. Variation of asymmetry with proton energy.
Target thickness ○ = 12 keV at 500 keV; △ = 20 keV at 500 keV.

Fig. 5.1. Variation of asymmetry with proton energy. Target thickness O = 12 Kev; △ = 20 Kev. (After Devons and Hine; De 49).

gamma rays at 15° and 145°. Their experimental results are shown in figure 5.1 and this is to be compared with figure 4.7.

The two curves show the rapid change of the phase angle ($\delta$) between the resonant radiation and the non-resonant radiation of odd parity. The interference term is zero (and $\delta = \pi/2$) at $E_p = 434 \pm 3$ Kev in the present work and $433 \pm 2$ Kev in figure 5.1.

The results disagree in the position and value of the maximum anisotropies, I, of $W(\theta)_{14.8 + 17.6}$. In the present work, these occur at $E_p = 560$ (I = 1.8) and (380 Kev (I = 0.6) and in figure 5.1, they are at $E_p = 575$ (I = 2) and 350 (I = 0.55). The maxima of figure 5.1 are between those of $W(\theta)_{17.6}$ and $W(\theta)_{14.8 + 17.6}$ in the present work. It is possible that the geiger counter detector system used by Devons and Hine was more sensitive to the 17.6 Mev gamma ray and this is suggested by the value of the intensity ratio at the 441 Kev resonance which is twice as large as the present measurement.

On the assumption that the 441 Kev resonance was due to s-wave proton capture, Devons and Hine (De 49) were able to attribute the interference to a broad, even parity level of $Be^8$ associated with $Li^7(p,\alpha)\alpha$ reaction, which is resonant at 3 Mev, and to fit their

experimental curve to a theory based on the overlap of these two levels.

With the more recent evidence that the resonances are p-wave (De 50, De 54) there is no known overlapping odd-parity level of $Be^8$ which can give rise to the interference, but Wilkinson has suggested the interference could be due to odd-parity, direct s or d-wave proton capture.

A theoretical analysis of interference between the levels of $Be^8$ and a direct proton capture mechanism without a well-defined intermediate state is the subject of investigation by other workers (Br 60) and is limited, at the moment, to the simpler case of the ground state transition in the region of the 441 Kev resonance. The interfering radiation is assumed to be electric dipole from direct s-wave proton capture. The interpretation of the interference with the 14.8 Mev gamma ray is complicated by the undetermined mixing ratio of M1 and E2 radiation at the resonance.

At the 1030 Kev resonance, both gamma rays show interference effects and this provides additional evidence that they are both resonant at this proton energy. Both s and d-wave proton capture in the background contribute to the interference with the p-wave resonance. It is also possible that there is a p-wave component in the background giving rise to cos $\theta$ terms

in the background radiation itself. The theoretical analysis of the mechanisms which give rise to the observed variation of the coefficient of cos θ at this resonance would be difficult, but an extension of the measurements to higher proton energies may assist the interpretation.

4. Conclusions.

In the light of the evidence that the 441 and 1030 Kev resonances are p-wave, we may summarise the conclusions from the present investigation of the $Li^7(p,\gamma)Be^8$ reaction.

1. The two gamma rays from the 441 Kev resonance are isotropic and consistent with the resonance being p-wave with channel spins 1 and 2 in the ratio of $1/5$.

2. Both gamma rays are resonant at the 1030 Kev resonance. The angular distributions of the resonance radiation have not been measured accurately and they do not lead to any definite conclusions on the mechanism of the 1030 Kev resonance. The results are not inconsistent with the resonance being p-wave ($J = 1^+$) with channel spins 1 and 2 in the ratio of $1/5$.

3. The non-resonant background between the 441 and 1030 Kev resonances includes both s and d-wave proton capture radiation. Interference between the two gives rise to significant $a_2$ terms in the angular distributions. The value of $a_2$ is approximately the same for both gamma rays.

4. The separation of the two gamma rays corresponding to transitions to the ground state and first excited state of $Be^8$ has shown their respective angular distributions to differ markedly in the neighbourhood of the 441 and 1030 Kev resonances as a result of the interference between the resonant, even parity states and proton interactions of opposite parity.

4.1. Further Work.

It is unfortunate that the present measurements could not be extended to higher proton energies; the information on the 1030 Kev resonance is incomplete and a more precise measurement of $a_2$ up to $E_p$ = 1.5 Mev would be useful in the interpretation of the resonance and the non-resonant background.

The investigation of the 2.1 Mev resonance in the $Li^7(p,\gamma)Be^8$ reaction has been limited to the measurement of excitation functions of the unresolved gamma rays at 0° and 90° (Pr 54, Ne 57). The latter workers also,

measured the intensity ratio of the components at 120° to the proton beam and found only the 14.8 Mev component to be resonant. If, as has been shown at the 1030 Kev resonance, the intensity ratio is a strong function of the angle of observation, their conclusion may be wrong. An angular distribution measurement at this energy would be of interest.

Finally, there is clearly a need for a $(\gamma-\alpha)$ angular correlation measurement of the 14.8 Mev gamma at the 441 Kev resonance in order to determine the mixing ratio of M1 and E2 radiation in this component. A knowledge of this ratio is required to explain the marked difference in the interference term in the 17.6 Mev and 14.8 Mev components.

# PART B.

## CHAPTER VI.

## Studies in Photodisintegration.

Introduction.

The investigations presented in this section involve the application of techniques developed in this laboratory by Mann, Ophel and Wright (Ma 57, Op 58) for the measurement of photo-proton spectra in thin inorganic scintillators which serve as both target and detector. Using monochromatic gamma radiation from the $Li^7(p,\gamma)Be^8$ reaction, photo-protons have been resolved with a resolution as high as 5% and it has been possible to study the photodisintegration of the elements in the common inorganic scintillators: $Na^{23}(\gamma,p)Ne^{22}$ (Op 58); $K^{39}(\gamma,p)A^{38}$ (Op 59); $Cs^{133}(\gamma,p)Xe^{132}$ and $I^{127}(\gamma,p)Te^{126}$ (Wr 58). The measured cross sections and the energy distribution of the photo-protons can be compared with the predictions of the statistical theory to test the significance of the two possible reaction mechanisms: compound nucleus and direct proton emission.

2. Techniques in Photodisintegration Studies.

It is convenient to discuss briefly the methods used by other workers in this type of investigation so that the present method can be compared with them.

2.1. Residual Activation.

The measurement of photonuclear reaction cross sections by irradiating elements with gamma rays and

measuring the residual activation has been a widely-used technique in photodisintegration studies. Details of the investigation are within the scope of a review article by Strauch (St 53). The method does not allow the investigation of particle spectra, but measurement of excitation functions, using betatrons and electron synchrotrons, have established the general features of the giant resonance in photonuclear reactions (Mo 53) and it is often possible to compare the cross-sections of $(\gamma,n)$, $(\gamma,p)$, $(\gamma,2n)$ and $(\gamma,3n)$ reactions in one target to distinguish between compound nucleus and direct emission processes. (Ca 57, Hi 47). Since many $(\gamma,p)$ reactions lead to stable products, the method is limited in its application, and direct observation of reaction products is necessary to extend the field of measurement.

2.2. Charged Particle Spectroscopy.

The spectroscopy of photo-nuclear reactions has been limited to charged particle emission in $(\gamma,p)$, $(\gamma,d)$ and $(\gamma,\alpha)$ reactions. The yield from an irradiated target has been observed by an array of photographic plates surrounding the target (To 51) or by scintillation counters (Lo 59) and angular distributions have been measured in this manner. For an adequate yield, the measurements require an intense collimated gamma ray

beam and this type of investigation has been limited to betatron and synchrotron sources where the details of the energy spectra are smeared by the continuous energy spread of the bremsstrahlung.

More precise measurements of the energy spectra have been made by investigating photo nuclear reactions in the detector medium. For discussion, these may be divided into four groups:

a. Nuclear Emulsions.

The use of nuclear emulsions in the investigation of photodisintegration has been reviewed by Titterton (Ti 55). Measurements have been made by irradiating emulsions loaded with a number of light elements. In general the spectra are more easily interpreted when monochromatic gamma ray sources from proton capture in light nuclei have been used. Where emulsions have been irradiated with bremsstrahlung, it is sometimes possible to calculate from the measurement of the tracks in each event in the emulsion, the energy of the incident gamma ray. An excitation function can be derived from the energy distribution of gamma rays in the bremsstrahlung. Resonant absorption peaks have been found in this manner in $C^{12}(\gamma,3\alpha)$ and $O^{16}(\gamma,4\alpha)$, (Go 53), $Li^{7}(\gamma,t)He^{4}$ (Ti 53) and $B^{10}(\gamma,d)2\alpha$ (Mu 52).

Energy spectra of 5 - 20% resolution have been obtained by irradiating nuclear emulsions with monochromatic gamma rays from the $Li^7(p,\gamma)Be^8$ and $F^{19}(p,\gamma,\alpha)O^{16}$ reactions. (Na 52a, Wa 53) and it is possible to measure angular distributions of the reaction products in the emulsion. The technique has extended the field of measurement considerably but the accumulation of data is tedious and other methods have been sought to eliminate the visual measurement of tracks and to improve the overall statistical accuracy.

b. Cloud Chambers.

Cloud chambers have been filled with helium (Ga 51) and nitrogen (Wr 57) to study the $He^4(\gamma,p)H^3$ and the $(\gamma,p)$, $(\gamma,n)$ and $(\gamma,\alpha)$ reactions in $N^{14}$ using bremsstrahlung. The $H^2(\gamma,p)n$ reaction has been investigated using the 6.1 Mev gamma rays from $F^{19}(p;\gamma,\alpha)O^{16}$. (Ph 50). The density of the detector medium is low and for a reasonable statistical accuracy very long running times are required with the most intense gamma ray beams that are available.

c. Proportional Counters.

Proportional counters filled to a few atmospheres of pressure with a number of suitable

gases have been irradiated with monochromatic gamma rays, generally from the $Li^7(p,\gamma)Be^8$ reaction, and the photodisintegration of the counter gas has been studied as in $H^2(\gamma,p)n$ (Ba 52); $C^{12}(\gamma,3\alpha)$, (Ca 55); $N^{14}(\gamma,p)C^{13}$, $N^{14}(\gamma,\alpha)B^{10}$, $Ne^{20}(\gamma,\alpha)O^{16}$ and $Ne^{20}(\gamma,p)F^{19}$, (Ha 60); $A^{40}(\gamma,p)Cl^{39}$, (Wi 51). Discrete particle groups have been resolved in the reactions, with the exception of the first two, where levels of the residual nucleus are not involved, and transitions to levels in the residual nucleus have been identified. The method is limited by the number of suitable counter gases available; the resolution of the counters (10 - 20% ) and the long decay time of the pulse output from the counter which limits the counting rate.

2.3. Summary.

Most of the information available in a systematic study of photodisintegration has come from experiments using the activation technique which only allows the measurement of cross sections and excitation functions. A knowledge of the energy and angular distributions of reaction products is needed for an exact interpretation of the reaction mechanism. These parameters must be

determined using monochromatic gamma ray sources and detectors with good energy resolution. To date, few measurements of this type have been made which allow a detailed comparison with theory, the notable exception being the photodisintegration of the deuteron.

2.4. The Present Method.

The use of inorganic scintillators as both target and detector is an extension of methods discussed in sections 2.2 a, b and c but there are a number of advantages in this method namely:

1. The density of the target material is higher than that used in proportional counters and nuclear emulsions. The inorganic scintillators do not require elaborate preparation.

2. The small size of the detector and mounting allows it to be placed close to weak monochromatic gamma ray sources.

3. By a suitable choice of crystal dimensions, the detector can be made relatively insensitive to the gamma ray flux traversing it.

4. The fast decay times of inorganic scintillators allow fast counting rates without pile-up of small pulses from electron-pairs traversing the crystal.

5. The energy resolution of inorganic scintillators is at least a factor of two better than that of proportional counters and equal to or better than that attained with nuclear emulsions.

Against these advantages, two disadvantages of inorganic scintillator target-detectors can be stated:

1. The target-detector system is not readily used in the measurement of angular distributions of the reaction products.

2. Inorganic scintillators include at least two isotopes and the particle spectra cannot always be interpreted unambiguously. In the case of the common scintillators NaI(Tl), KI(Tl) and CsI(Tl), apart from the low percentage of thallium activator, only two isotopes are present (with the exception of potassium which is in any case 93% $K^{39}$). The low cross section of the $I^{127}(\gamma,p)Te^{126}$ reaction and the fact that this reaction is common to the three scintillators allows a separation of the reaction products from $I^{127}(\gamma,p)$ and $Na^{23}(\gamma,p)$, $K^{39}(\gamma,p)$ (Op 58) or $Cs^{133}(\gamma,p)$ (Wr 58).

## 2.5. Presentation of Material.

The remainder of this chapter is devoted to a description of experimental techniques used in the study of the $Na^{23}(\gamma,p)Ne^{22}$ and $Br^{79,81}(\gamma,p)Se^{78,80}$ reactions in

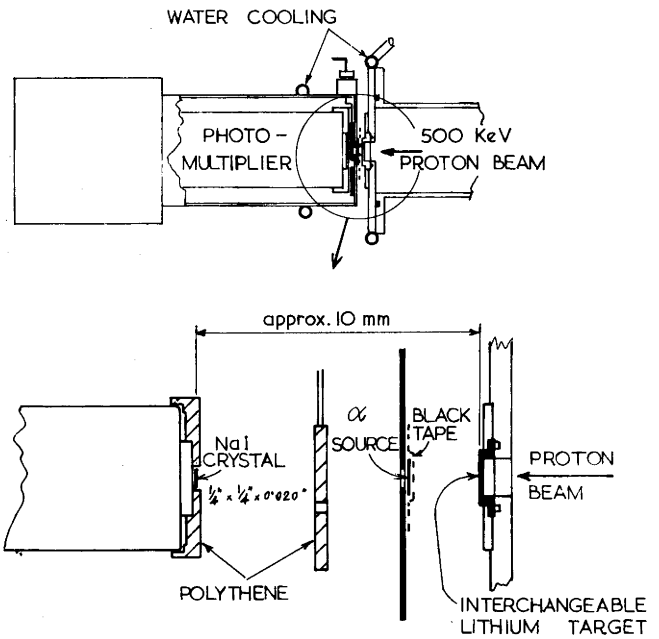


Fig. 6.1. Scintillation counter used for studying $(\gamma,p)$ reactions in inorganic scintillators.

NaI(Tl) and Cs Br(Tl) scintillators. The techniques used in these experiments have been described by Ophel and Wright (Op 58) and for this reason are only presented briefly. The experimental results of the present measurements are reported in Chapter VII.

3.1. The Counter Assembly.

Thin crystals of inorganic scintillators were irradiated with gamma rays from the $Li^7(p,\gamma)Be^8$ reaction at the 440 Kev resonance. The apparatus used is shown in figure 6.1. The thin crystal, mounted on a 1/8 in. perspex disc is optically sealed to the E.M.I. photomultiplier tube, type 6097 F. The crystal is surrounded with polythene sufficiently thick to stop external photoprotons from reaching the target-detector.

The front polythene cover is in the form of a movable shutter which can be moved between runs to admit alpha particles from a thin ThC + ThC' source mounted behind the shutter. This is necessary to maintain a check of the gain of the system during long periods of irradiation.

3.2. Electronics.

Pulses from the cathode follower built into the photomultiplier base were amplified by a linear amplifier and fed to a Hutchinson-Scarrott type multichannel pulse height analyser. The analyser was found not to be

linear for pulses of rise time shorter than 1μ sec. and for this reason, a simple pulse integrating circuit was included in the cathode follower to increase the rise time of the pulses to 2μ sec.

3.3. Gain Variation.

An inherent fault in photomultiplier tubes is that the gain of the detector varies when it is under a fast counting rate (Be 55, Ev 54). The explanation of this behaviour involves surface effects on the dynodes of the photomultiplier. It has been found in this work that the drift is more noticeable in a new tube and that the stability of the detector improves with continual use. Variations of up to 30% in gain were observed in the first hours of running but after fairly constant use, this variation was normally of the order of $\pm$ 2% every half hour.

In these experiments, where long running times are involved, a drift of 2% in gain in half an hour can affect the resolution of the experiment, and for this reason, a thin ThC + ThC' source giving alpha particles of 8.8 Mev and 6.0 Mev was incorporated in the front of the detector and covered with a 0.1 in. thick polythene shutter when not in use. The spectrum from the kick-sorter was recorded every half hour and the shutter was removed to admit the alpha particles. By setting the

gain so that the peak of the 8.8 Mev alpha spectrum fell between two adjacent channels of the kicksorter, it was possible to observe a gain shift as small as $\pm$ 1/2% and the bias to the photomultiplier dynodes was adjusted to compensate for the drift.

4.1. Crystal Preparation.

The crystals were cut to their approximate size (generally 1/4 in. x 1/4 in. x 0.150 in.) with a fine jeweller's saw. A fine weave cotton cloth was stretched over a flat glass plate and one side of the crystal was polished by wetting the cloth with a 1% solution of glycerol in distilled water and rubbing the crystal face on the wet surface. The polished crystal was dried with absorbent paper and cemented to a standard 1/8 in. thick perspex disc machined to the shape of the window of the photomultiplier. The cement used was Araldite type 101. It forms a transparent film under the crystal with good optical contact between the two surfaces. By carefully pressing the crystal to push out small air bubbles, it is possible to form an Araldite film 0.0005 in. thick.

After the cement had set, the perspex disc was mounted in a brass holder with a variable recess which was adjusted with a micrometer depth gauge to about 0.003 in. greater than the required crystal depth.

The crystal was rubbed down on the wet rubbing plate until the brass holder fouled on the plate. This ensured that the rubbing produced a crystal with uniform depth. The last few thousandths of an inch were removed by rubbing with the disc held in the hand. It was possible to prepare a crystal of the specified thickness to within 0.0005 in.

In the case of sodium iodide which is hygroscopic, the crystal preparation was carried out in a dry box, acetone being used instead of water for the final polish. Before removing the crystal from a dry box, it was covered with a thin smear of vaseline and the whole was covered with a 1.5 mg./cm.$^2$ aluminium foil which was pressed down firmly over the crystal. This was sufficient to protect the crystal in normal atmospheric conditions and it remained in good condition for up to three weeks when the cemented surface becomes cloudy because of some reaction between the Araldite and the sodium iodide. Presumably this reaction is due to a small water content in the cement.

It was not necessary to cover crystals which are not hygroscopic and it is questionable if the aluminium reflector improved the resolution of the system significantly.

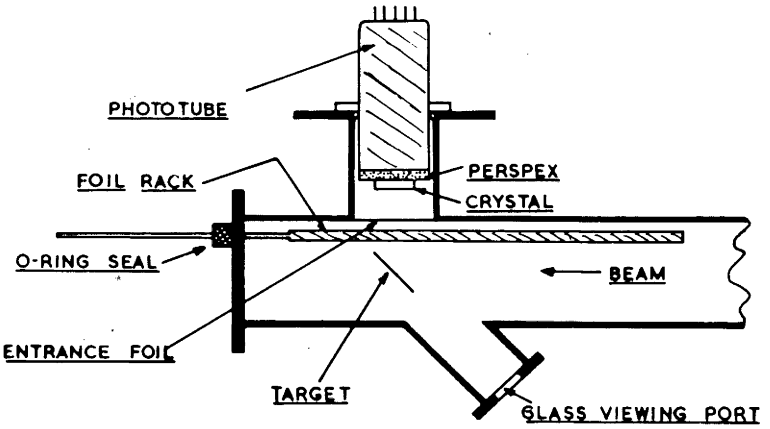


Fig. 6.2. The experimental arrangement used in the comparison of the proton, alpha and electron response of CsBr(Tl).

Apart from the convenience of mounting the crystal on a disc which can be easily sealed to the phototube with Dow-Corning silicone fluid, the perspex disc serves as a short light pipe and alleviates the inherent non-uniformity of the photocathode by permitting the light from each flash to fall more nearly on the whole cathode surface.

## 4.2. Response of CsBr(Tl) to Protons, Alpha Particles and Electrons.

The relative response of CsBr(Tl) to protons, alpha particles and electrons was measured in the target chamber shown in figure 6.2.

Protons from the $B^{10}(d,p)B^{11}$ reaction were observed at 90° to the beam by a ¾ in. by ¾ in. by 0.1 in. CsBr(Tl) scintillation counter. A 1.5mg./$_{cm.}2$ aluminium window served as a light seal in front of the photomultiplier and 12.7 mg./$_{cm.}2$ and 34.8 mg./$_{cm.}2$ aluminium foils were mounted on the movable foil rack shown in the figure. It was possible to measure through the foils the response of the detector to proton groups between 3 and 9 Mev.

The ThC + ThC[1] alpha source mounted on the foil rack was used to monitor the gain during the measurements and the $\alpha$ spectrum was used to measure the response of CsBr(Tl) to alpha particles.

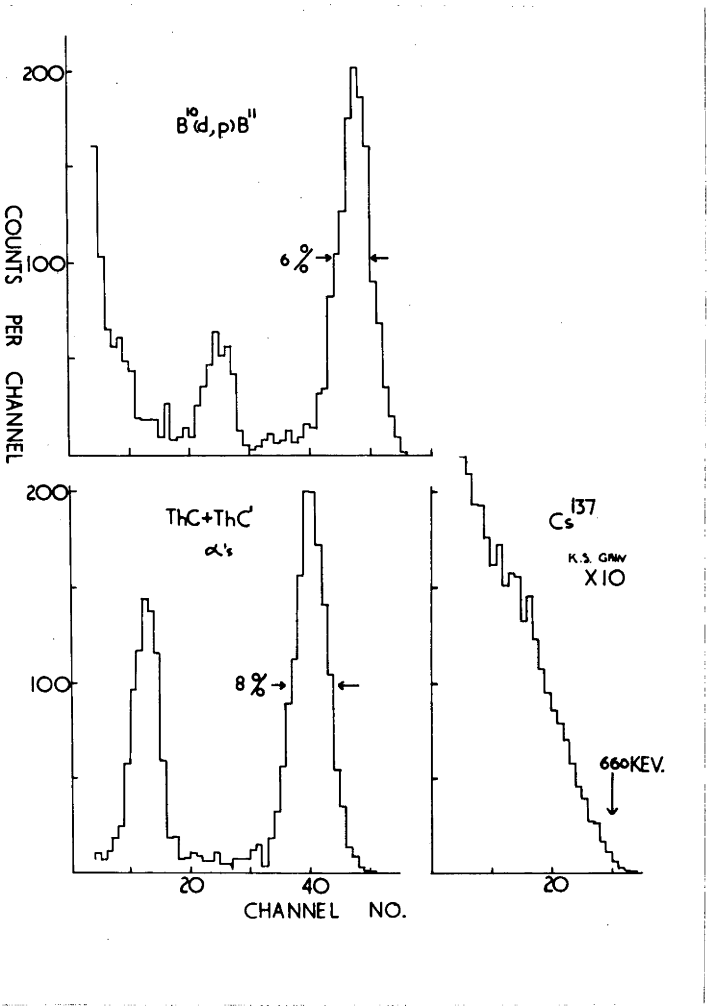


Fig. 6.3. Proton, alpha and gamma ray spectra for a 3/4in. x 3/4in. x 0.10 in. CsBr(Tl) scintillator.

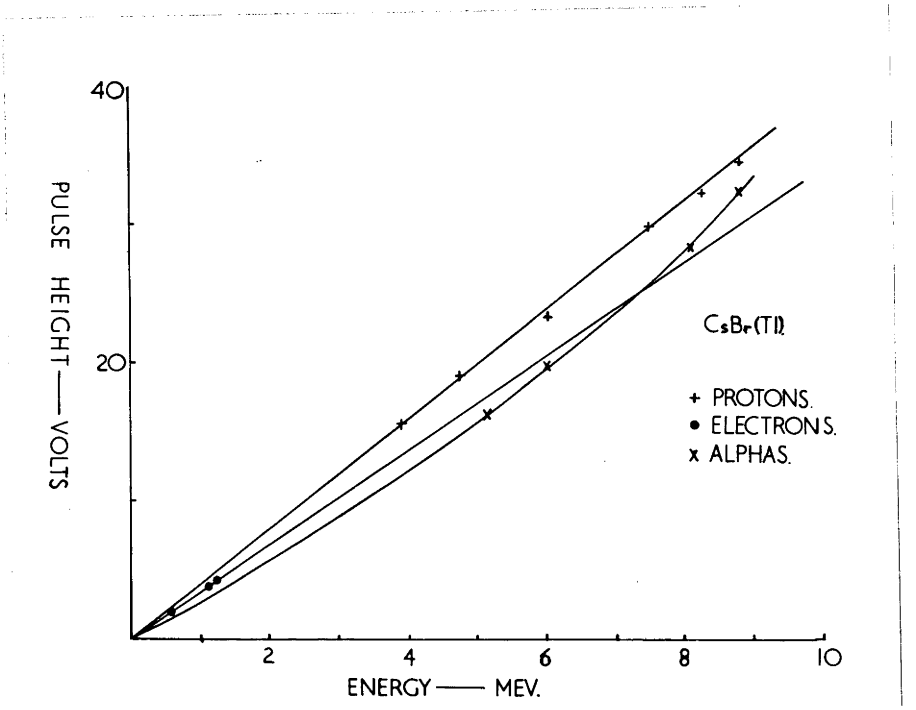


Fig. 6.4. The relative response of CsBr(Tl) to protons, electrons and alpha particles.

The output from the photomultiplier was amplified and fed to a 100-channel pulse height analyser. A thin target of natural boric oxide was bombarded with 600 Kev deuterons and proton spectra were measured through the 1.5 mg./$_{cm.2}$ , 14.2 mg./$_{cm.2}$ and 36.3 mg./$_{cm.2}$ foils.

Immediately after the deuteron bombardment, 2μ Curie sources of $Cs^{137}$, $Zn^{65}$ and $Na^{22}$ were placed adjacent to the crystal but outside the target chamber. The spectra were recorded with the gain of the pulse height analyser set to the X10 scale.

Figure 6.3 shows typical spectra obtained in the comparison. No gamma ray line was resolved but the end-point of the $Cs^{137}$ spectrum is due to 660 Kev electrons being completely stopped in the crystal.

The pulse height of the ∝,p and e groups were measured from a voltage calibration of the analyser and are plotted against particle group energy in figure 6.4†. The two extra points on the ∝ response curve were obtained by removing the 1.5 mg./$_{cm.2}$ aluminium window.

In figure 6.3, the energy resolution of CsBr(Tl) is of the order of 6 - 8% which is slightly worse than

---

† It must be noted that scintillation counter pulse shapes for ∝, p and e differ (St 58[8], Ow 59) and the relative response depends on the integrating circuits used in the electronics.

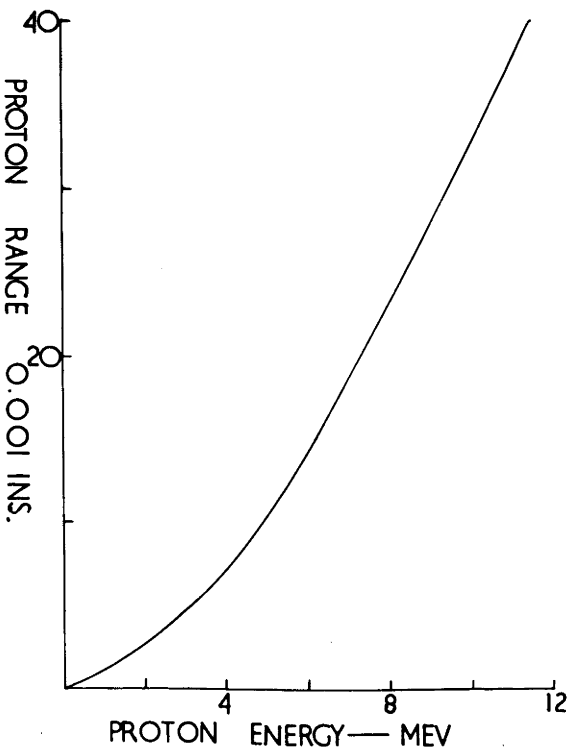


Fig. 6.5. Range-energy relation for protons in CsBr.

the 4 - 5% resolution of NaI(Tl) crystals (Op 58).

4.3 Range of Protons in CsBr(Tl).

Approximate range-energy curves for protons in caesium and bromine were obtained from a plot of proton range against atomic number for a number of proton energies up to 12 Mev taken from the data of Aron et al. (Ar 51) for aluminium, copper, silver and lead.

These were used to estimate the proton range-energy curve (figure 6.5) for caesium bromide by the Bragg-Kleeman empirical rule

$$\frac{R\rho}{\sqrt{A}} = \text{constant},$$

where R is the range of a proton of given energy in a material of density $\rho$ and atomic weight A. By this rule, the atomic weight of CsBr is written as

$$\sqrt{A} = \sqrt{A_{Br}} + \sqrt{A_{Cs}}. \qquad \text{(Ev 55)}.$$

4.4 Correction for Loss of Protons from the Detector.

For isotropic, monoenergetic particles of range R in a layer of infinite extent and thickness 2d, the fraction f, of particles completely stopped in the layer is given by:

$$f = \left(1 - \frac{R}{4d}\right) \quad \text{for} \quad R < 2d$$

$$f = \frac{d}{R} \quad \text{for } R > 2d \qquad \text{(Gr 48)}.$$

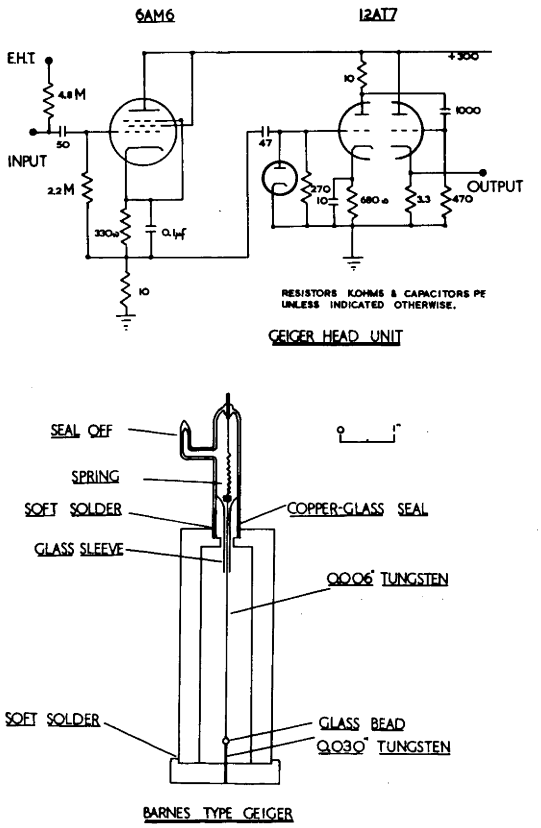


Fig. 6.6. The Barnes-type thick-walled geiger counter.

5. The Gamma Ray Source.

Both resonance and non-resonance radiation from the $Li^7(p,\gamma)Be^8$ reaction was used as a gamma ray source. Thick targets were prepared by the evaporation of natural lithium metal onto standard copper backings 0.040 in. thick. The targets were transferred from the evaporator to the target assembly in less than one minute without any apparent deterioration of the deposit. For resonance radiation, targets 200 Kev thick were bombarded with 500 Kev protons with currents up to 150μA. When non-resonance radiation was used, the targets were limited to a 150 Kev thickness and the proton energy was 850 Kev. Under these conditions, the intensity ratio of the 14.8 and 17.6 Mev components of the radiation was $\frac{I\ 17.6}{I\ 14.8}$ = 1.8 at $E_p$ = 500 Kev and approximately 0.6 at $E_p$ = 850 Kev in the forward direction (Chapter III). The resonance radiation was assumed to be isotropic.

5.1 Gamma Ray Monitor.

Three thick-walled Barnes-type (Ba 52) geiger counters shown in figure 6.6 were first used to monitor the gamma ray beam. These have a sensitivity of 2.66 counts/qantum/$cm^2$ for 17.6 Mev gamma rays and 2.1 counts /qantum/$cm^2$ for 14.8 Mev Gamma rays (Ba 52). The counters were found to have a limited useful life which

was believed to be caused by outgassing of the brass walls. They were replaced by commercial glass-walled geigers with a normal argon-alcohol filling and mounted in brass cylinders with the dimensions of the Barnes geigers. The sensitivity of the two types was compared and found to be identical (Wr 58).

The pulse output from the geiger monitors was counted on Harwell-type 1008 scalers with a dead time of 200μ sec. Three monitors were placed at convenient positions 1.5 metres from the target and at this distance, the counting rate was low enough to limit counting losses to 1%.

## 6. Irradiation of the Scintillators.

This section includes a short discussion of the measurement and interpretation of the spectra observed in the irradiation of the scintillators by gamma rays.

### 6.1. Electron Background.

The proton and electron response curves for CsBr(Tl) are similar, and in order to detect protons in the presence of the high energy gamma ray flux, the crystal dimensions must be too small for high energy electrons to lose much of their energy in the scintillator, but large enough to stop a 12 Mev proton. Since electron pairs are projected in the forward direction, the height of the electron pulses would be primarily a function of

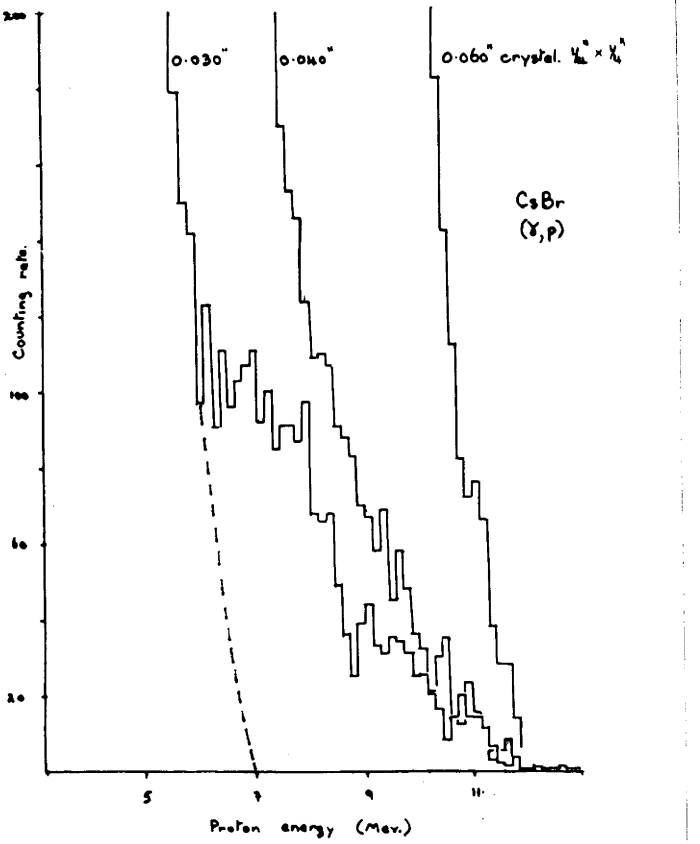


Fig. 6.7. The position of the electron background in 1/4in. x 1/4in. CsBr(Tl) crystals of varying thickness.

the crystal depth, but larger pulses would arise from electrons scattered along the crystal or by pile-up of a number of small pulses.

Figure 6.7 shows spectra from a $^1/_4$ in. x $^1/_4$ in. CsBr(Tl) crystal irradiated with resonance radiation from $Li^7(p,\gamma)Be^8$. The crystal depth was reduced in stages from 0.060 in . to 0.040 in. and 0.030 in, and the gain of the system was not altered during the comparison. The pulse height of the electron edge extends to a proton energy of about 12 Mev for the 0.060 in. crystal, and with the reduction of the depth, the proton spectrum emerges from the electron background. In practice it was found that a $^1/_4$ in. x $^1/_4$ in. x 0.025 in. CsBr(Tl) crystal allowed the measurement of the proton spectrum beyond 6 Mev. This is in contrast with the alkali iodides where the workers were able to measure the proton spectrum in a crystal of the same dimensions from 3 Mev upwards. (Op 58, 59).

6.2. Pile Up.

Because of the high counting rate in the electron background during irradiation, addition pulses can occur in the scintillation counter output but the effect was considered negligible for the following reasons:

1. The shape of the electron background was found to be independent of the intensity of the gamma ray flux,

2. No difference in the shape of the ThC + $ThC^1$ alpha particle spectrum was observed with the gamma ray beam on or off.

6.3. Competitive Reactions.

The scintillator was surrounded with a polythene envelope thick enough to stop 15 Mev protons. The only source of competitive reactions outside the crystal was the polythene, Araldite, Perspex and the thin aluminium foil used to protect hygroscopic crystals. The threshold for $C^{12}(\gamma,p)$ is 15.95 Mev and 1.7 Mev photo-protons from this reaction would appear in the electron background. Photo-protons from oxygen in the perspex and the aluminium foil were unavoidable but their contributions were assumed to be negligible.

Competitive reactions such as $(\gamma,\alpha)$ and $(\gamma,d)$ in the crystal are detected, but since their cross sections are generally of an order of magnitude less than $(\gamma,p)$ reactions, the yield is relatively small.

6.4. Energy Calibration.

The photo-proton spectra were calibrated by comparison with the proton groups from the $B^{10}(d,p)B^{11}$ reaction using the same crystal in both experiments and maintaining the same gain setting of the electronics.

The apparatus used is shown in figure 6.8.

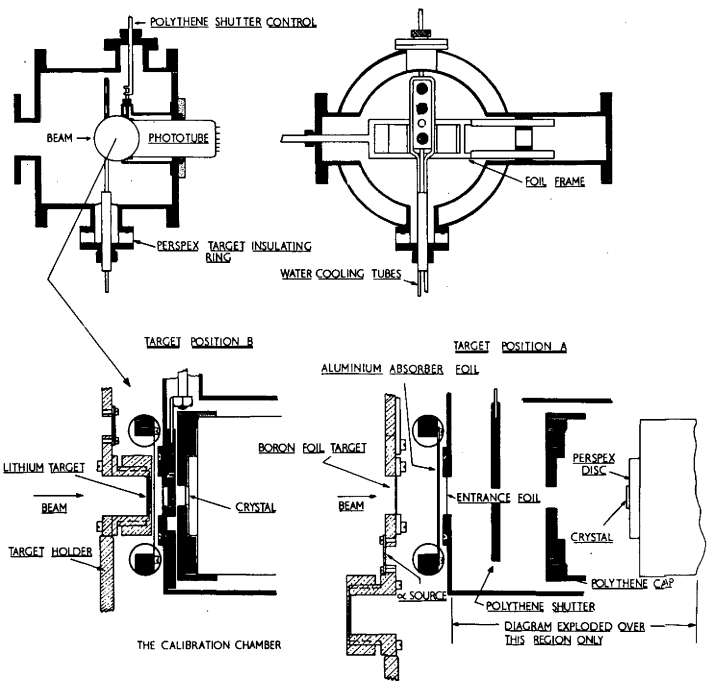


Fig. 6.8. The calibration chamber for comparing $(\gamma,p)$ spectra with the $B^{10}(d,p)B^{11}$ reaction.

Essentially, the detector assembly is the same as in figure 6.1 but it was placed in a vacuum and covered with a brass "hat" containing a thin aluminium window to admit external protons from the boron target when the polythene shutter is open. The protons were detected at 0° through a 1.5 mg./$_{cm^2}$ Al target backing and a series of aluminium foils could be set between the target and scintillator to provide lower energy calibration points.

After detecting the (d,p) reaction, a thick lithium target was moved into position and bombarded with 500 Kev protons to obtain a ($\gamma$,p) spectrum from the crystal. The ThC + ThC$^1$ alpha source which was used to monitor the gain shift during the experiment was mounted on the back of the polythene shutter which could be moved into three positions: for a gain check, to admit external protons to the detector, and to cover the crystal during the ($\gamma$,p) run.

# CHAPTER VII.

## ($\gamma$,p) Reactions in NaI(Tl) and CsBr(Tl).

Introduction.

The measurement of $(\gamma,p)$ reactions in NaI(Tl) and CsBr(Tl) inorganic scintillators are described in this chapter. The apparatus, gamma ray source and experimental method are common to both investigations and have been described in chapter VI.

1. The $Na^{23}(\gamma,p)$ Reaction at 14.8 and 17.6 Mev.

An investigation of this reaction in NaI(Tl) crystals was first reported by Ophel and Wright (Op 58) who used $Li^7(p,\gamma)Be^8$ radiation as a gamma ray source. The radiation includes two components of energy 17.6 and 14.8 Mev (2 Mev broad) whose intensity ratio is known to vary with proton energy (Wa 48). In the energy region where proton groups from the 14.8 Mev component are possible, the $(\gamma,p)$ groups due to the 14.8 and 17.6 Mev components have been identified from a comparison of photo-proton spectra obtained with resonance and non-resonance radiation.

Figure 7.1 shows proton spectra measured by Ophel and Wright from a $\frac{1}{4}$ in. x $\frac{1}{4}$ in. x 0.018 in. NaI(Tl) crystal using resonance and non-resonance radiation. The gain of the detector and pulse height analyser were kept constant in the experiment and the two spectra have been normalised to the same number of monitor counts.

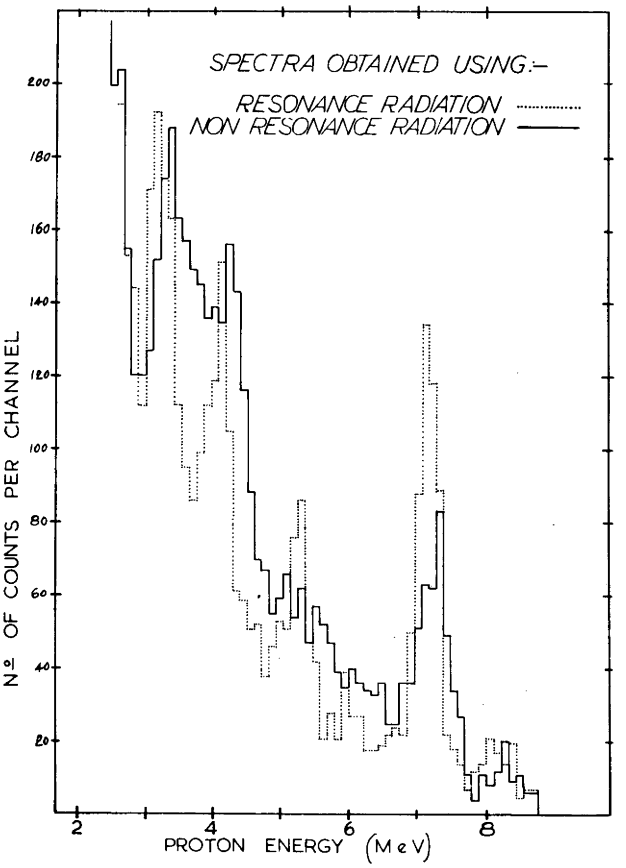


Fig. 7.1. Comparison of the $Na^{23}(\gamma,p)Ne^{22}$ spectra obtained using resonance and non-resonance radiation.
(After Ophel and Wright, Op 58).

These workers were able to attribute the proton groups at 3.2, 4.1, 5.2, 7.2 and 8.4 Mev to transitions through the 5.4, 4.4, 3.3, 1.3 and 0 Mev levels of $Ne^{22}$ for the 17.6 Mev component for the following reasons:

1. Being a sharp gamma line, the 17.6 Mev component will give a corresponding increase in the energy of the proton groups for non-resonance radiation. On the other hand, the 14.8 Mev component is approximately 2 Mev broad (Wa 48) and if it produces sharp proton groups at all, they must arise from selective absorption of a narrow energy range of the broad component. The increase in the energy of the broad component for non-resonance radiation will not therefore give rise to an increase in proton energy.

2. The intensity ratios of the two components differ in resonance and non-resonance radiation. If a resonance and non-resonance spectrum are compared after normalising the two to the same number of geiger counts, the intensity of the proton groups due to the 17.6 Mev component should be reduced by a factor of 1.6 in the non-resonance spectrum, if one allows for the different response of the monitor to the two gamma rays.

In comparing the two spectra of figure 7.1, Wright and Ophel concluded that the number of counts in the groups at 4.2 and 3 Mev was reduced in the non-resonance spectrum, but the peaks were lifted by an increase in an underlying broad group centred at about 4 Mev, corresponding to the transition through the 1.3 Mev level of $Ne^{22}$ for 14.8 Mev radiation.

The investigation reported in the following section was performed to re-examine the latter conclusion.

1.1. <u>A Comparison of the $Na^{23}(\gamma,p)Ne^{22}$ Spectra with Resonance and Non-Resonance Radiation from $Li^{7}(p,\gamma)Be^{8}$.</u>

A $\frac{1}{4}$ in. x $\frac{1}{4}$ in. x 0.025 in. NaI(Tl) crystal was prepared and mounted in the manner described in chapter VI and covered with a thin layer of vaseline and a 1.5 mg./$_{cm.2}$ aluminium foil to protect the crystal from water vapour. The experimental arrangement is shown in figure 6.1.

A 150 Kev thick lithium target was bombarded with 500 and 850 Kev protons with beam currents up to 120 μA. The gamma ray flux was monitored by geiger counters placed at 0°, 80° and 130° to the proton beam. The gain of the detector was kept constant during the resonance and non-resonance runs and was monitored by

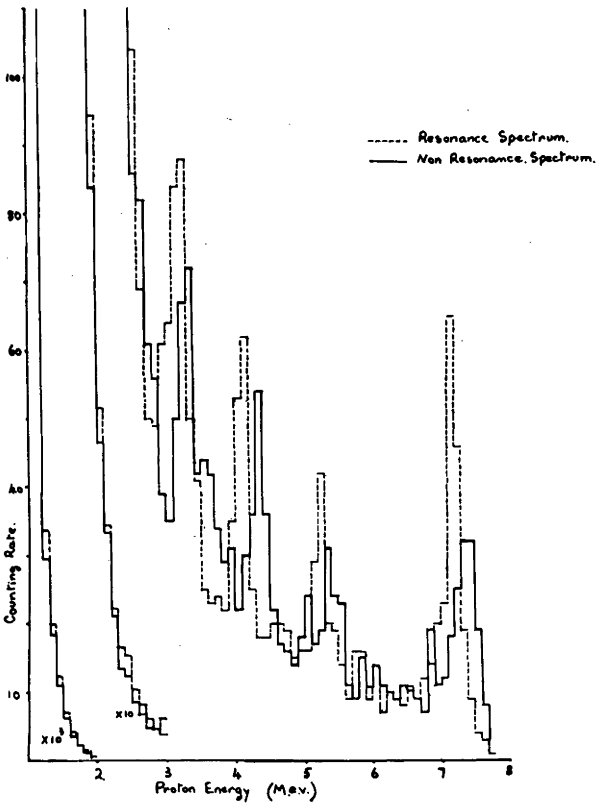


Fig. 7.2. Comparison of the $Na^{23}(\gamma,p)Ne^{22}$ spectra obtained using resonance and non-resonance radiation in the present measurements. Resonance running time 2-1/2 hours. Non-resonance running time 9 hours.

the ThC + $ThC^1$ $\alpha$ source at half-hourly intervals after recording the proton spectrum.

1.2. Results.

Figure 7.2 shows the spectra obtained in the two irradiations normalised to the same number of 0°- monitor counts. The energy scale is based on the calibration of Ophel and Wright (Op 58). The 8.4 Mev proton group was not of interest in this comparison and was not recorded.

The number of counts in each group of the resonance spectrum is greater than the non-resonance spectrum by a factor of about 1.4 and the energy shift of the four proton groups leads to the conclusion that they are due to the 17.6 Mev component. There is no evidence for the broad group at about 4 Mev which can be attributed to the 14.8 Mev component and this disagrees with the conclusion of Ophel and Wright (figure 7.1). The non-resonance measurements were repeated but no evidence for contributions from the lower energy gamma ray could be found in the spectra. The present results have been discussed with Ophel and Wright who accept this evidence but it is difficult to account for the cause of such a marked disagreement in the measurements at 4 Mev.

## 2. (γ,p) Reactions in CsBr(Tl).

The measurement of (γ,p) reactions in this scintillator is complicated by the presence of three isotopes: $Cs^{133}$, $Br^{79}$ (50.5% abundance in natural bromine) and $Br^{81}$ (49.5% abundance). The (γ,p) reactions in CsI(Tl) have been measured by Wright (Wr 58) of these laboratories and it has been possible to separate the (γ,p) spectra for $Cs^{133}$ and $I^{127}$ by comparison with the measurements in KI(Tl) and NaI(Tl) (Op, 58,59). It is thus possible to separate the $Cs^{133}(\gamma,p)Xe^{132}$ contribution in the photo-disintegration of CsBr(Tl).

### 2.1. Experimental.

The preparation of the phosphor and the experimental procedure followed in the photodisintegration measurements have already been described in earlier sections. It was at once apparent in the irradiation of CsBr(Tl) that the electron response of CsBr(Tl) relative to the proton response was higher than for the iodides (Chapter VI, 6.1). For a 1/4 in. x 1/4 in. x 0.030 in. crystal, the electron background was found to extend to a proton energy of 6 Mev and the position of the electron background was found to be relatively insensitive to crystal dimensions less than 1/4 in. x 1/4 in. x 0.020 in. These investigations were limited to

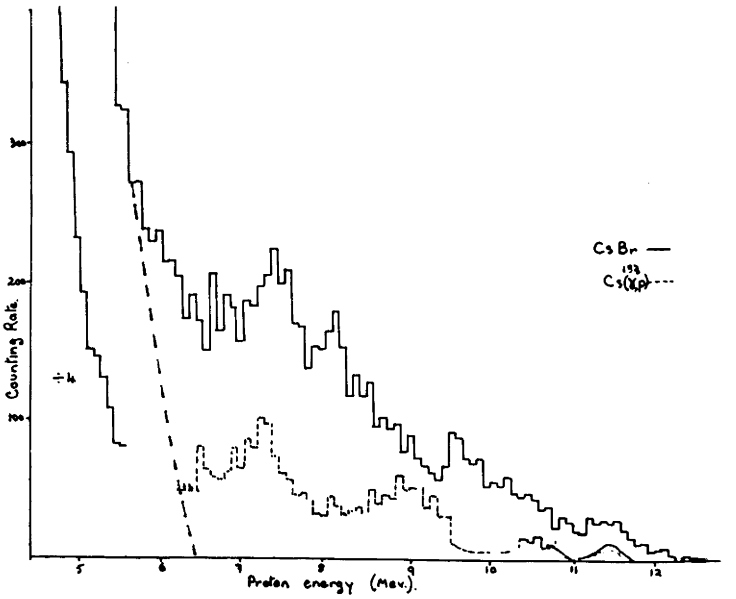


Fig. 7.3. $(\gamma,p)$ spectra observed in CsBr(Tl) and CsI(Tl) crystals 1/4in. x 1/4in. x 0.025in. for the same gamma ray flux. The CsI(Tl) spectrum has been corrected for contributions from the $I^{127}(\gamma,p)Te^{126}$ reaction. The electron background is that for CsBr(Tl).

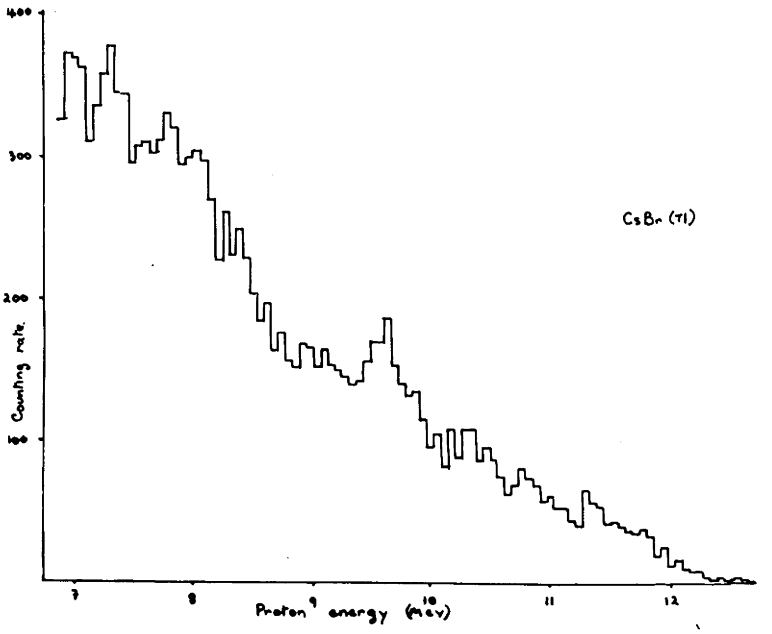


Fig. 7.4. $Cs^{133}$, $Br^{79,81}$ $(\gamma,p)$ spectrum. from crystal 1/4in. x 1/4in. x 0.030 in. Running time 5 hours.

the measurement of photo-protons of energy greater than 6 Mev.

2.2. Results.

Some fifteen separate runs were made irradiating CsBr(Tl) with resonance radiation. $\frac{1}{4}$ in. x $\frac{1}{4}$ in. crystals of thickness between 0.015 in. and 0.040 in. were used and the feature of all the spectra was the existence of a broad maximum about a proton energy of 7.6 Mev. Figure 7.3, 7.4 and 7.5 show typical spectra which are the sum of a number of pulse height distributions recorded at half-hourly intervals before each check on gain variations.

The spectra are all that one might expect from a target containing three isotopes and a detector with a resolution of 6 - 8 %. The broad peak about 7.6 Mev appears to include at least two proton groups but it has been impossible to resolve them with any convincing results. The only group which was resolved consistently was that between 9 and 10 Mev.

2.3. Energy Calibration.

An energy calibration of the $(\gamma,p)$ spectrum was obtained by comparing it with the proton spectrum of the $B^{10}(d,p)$ reaction in the manner described in chapter VI, section 6.4.

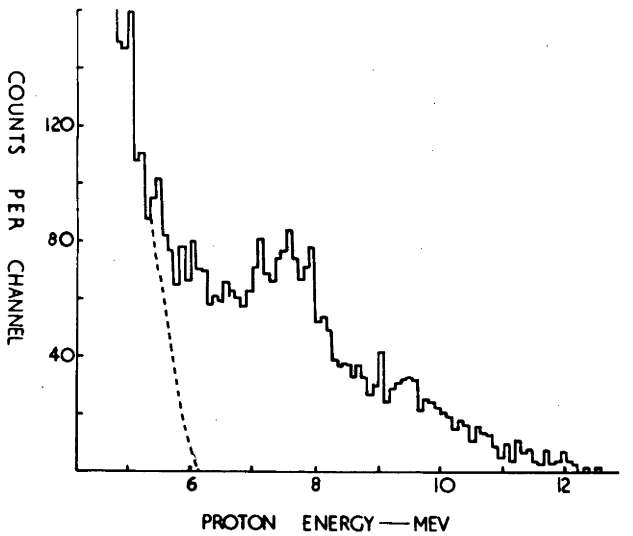


Fig. 7.5. $Cs^{133}$, $Br^{79,81}$ $(\gamma,p)$ spectrum from crystal 1/4in. x 1/4in. x 0.015 in. Running time 4 hours.

Two calibrations fixed the position of the maximum in the broad group at 7.6 ± 0.3 Mev and the energy of the group about 9.5 Mev at 9.6 ± 0.1 Mev.

2.4. The $Cs^{133}(\gamma,p)Xe^{132}$ Spectrum.

Crystals of CsI(Tl) and CsBr(Tl) of the same dimensions ($\frac{1}{4}$ in. x $\frac{1}{4}$ in. x 0.025 in.) were prepared and irradiated with lithium gamma rays in the target-detector assembly of figure 6.1. The gain of the detector system for the two measurements was adjusted so that the energy calibration of the display on the pulse height analyser allowed a direct comparison of the spectra. They are shown in figure 7.3 after normalisation to the same number of counts on the three Barnes-type geiger counters used to monitor the gamma ray flux. Photo-protons from the $I^{127}(\gamma,p)$ reaction have been measured by other workers (Wr 58) and these proton groups have been subtracted from the CsI(Tl) $(\gamma,p)$ spectrum of figure 7.3. The number of $Cs^{133}$ nuclei per unit volume is approximately the same in CsBr and CsI and the $Cs^{133}(\gamma,p)$ contribution to the CsBr(Tl) $(\gamma,p)$ spectrum approximates to the broken curve of figure 7.3. The energies of these proton groups have been given as 7.3, 8.16, 9.15, 10.68 and 11.5 Mev (Wr 58).

TABLE 7.1.

Possible Proton Groups in CsBr($\gamma$,p)

Spectrum for $E_\gamma$ = 17.6 Mev.

| $E_p$. Mev | Residual Nucleus. | Energy Level (Mev). | Reference. |
|---|---|---|---|
| 7.3 | $Xe^{132}$ | | (Wr 58.) |
| 8.16 | $Xe^{132}$ | | (Wr 58.) |
| 9.15 | $Xe^{132}$ | | (Wr 58.) |
| 9.59 | $Se^{80}$ | 0.65 | (Te 56.) |
| 9.88 | $Se^{78}$ | 0.615 | (Te 56, St 58) |
| 10.24 | $Se^{80}$ | 0 | (Wa 53.) |
| 10.59 | $Se^{78}$ | 1.32 | (St 58.) |
| 10.68 | $Xe^{132}$ | | (Wr 58.) |
| 11.2 | $Se^{78}$ | 0 | (Wa 53.) |
| 11.5 | $Xe^{132}$ | 0 | (Wr 58.) |

## 2.5. Identification of Proton Groups in CsBr(γ,p).

A summary of the levels of $Se^{78}$ and $Se^{80}$ which have been identified in the coulomb excitation of $Se^{78}$ and $Se^{80}$ (Te 56) and the β decay of $As^{78}$ (St 58) is included in table 7.1. The proton groups which may arise in (γ,p) reactions at 17.6 Mev in $Br^{79,81}$ are tabulated with the proton groups observed in $Cs^{133}(\gamma,p)Xe^{132}$ by Wright.

For the 17.6 Mev gamma ray, protons corresponding to transitions to the ground states of $Se^{80}$, $Se^{78}$ and $Xe^{132}$ are expected at 10.24, 11.2 and 11.5 Mev respectively (St 58, Wa 53, Wr 58). Although the group at 10.24 Mev is probably present, it has not been resolved. It is fairly clear that the broad group between 11.2 and 11.7 Mev corresponds to transitions to the ground states of $Se^{78}$ and $Cs^{133}$.

Energy-wise, it is not possible to attribute the proton group at 9.6 Mev to the 14.8 Mev component and it has not been observed in the $Cs^{133}(\gamma,p)$ spectrum. It is concluded that this group is due to the $Br^{81}(\gamma,p)Se^{80}$ reaction at $E_\gamma$ = 17.6 Mev which can proceed by way of the 0.65 Mev level of $Se^{80}$.

The small number of events above 12 Mev may be due to (γ,α) reactions in the scintillator. The proton and alpha response curves of figure 6.4 suggest that the response of a 12 Mev α is greater than a 12 Mev

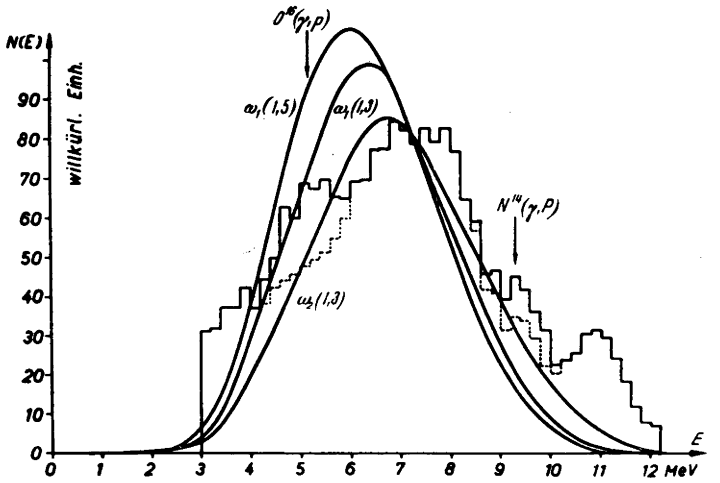


Fig. 7.6. Proton spectrum from photodisintegration of AgBr in a nuclear emulsion by $Li^7(p,\gamma)$ radiation.
(After Waffler, Wa 53).

proton and $\alpha$ particles of this energy have been observed in the $Br(\gamma,\alpha)$ reaction at 17.6 Mev (Na 52a).

2.6. AgBr($\gamma$,p) Reactions in Nuclear Emulsions.

Figure 7.6 shows a proton spectrum from the irradiation of a nuclear emulsion by lithium gamma rays reported by Waffler (Wa 53). The corrections for the $O^{16}(\gamma,p)$ and $N^{14}(\gamma,p)$ reactions in the emulsion are shown but the spectrum also includes contributions from the $(\gamma,p)$ reactions in $Br^{79}$, $Br^{81}$, $Ag^{107}$ and $Ag^{109}$. The interpretation is more complicated than the present measurements but the spectra have the same general features - a broad group about 7.5 Mev and a group which is partly resolved at 9.6 Mev. It would appear that the resolution of the spectrum from CsBr(Tl) is better but not precise enough to sort out the contributions from the three isotopes.

2.7. Cross Section Measurement.

The measurement of the cross section of the $CsBr(\gamma,p)$ reactions was based on the cross section ($2.5 \pm 0.1$ m.b.) of the transition to the 1.3 Mev level of $Ne^{22}$ in $Na^{23}(\gamma,p)\ Ne^{22}$ at 17.6 Mev reported by Wright and Ophel (Op 58).

This was done by irradiating $\frac{1}{4}$ in. x $\frac{1}{4}$ in. x 0.025 in. crystals of NaI(Tl) and CsBr(Tl) in the detector assembly of figure 6.1. By using crystals

of the same dimensions, it was possible to use the same geometry in both irradiations and avoid corrections for the dimensions of the gamma ray source which was defined by a 3/16 in.diameter beam stop immediately in front of the lithium target. The gamma ray beam was monitored by three thick-walled geiger counters 1.5m. from the target at 60°, 120° and 150°, and the two spectra were normalised to the same number of monitor counts.

The shape of the energy distribution of the electron background was taken from figure 6.7 and it was assumed as in figure 7.3 that the electron background in a 1/4in. x 1/4in. x 0.025 in. crystal does not extend beyond a proton energy of 6.5 Mev. It was also assumed that the photo-proton yield above this energy was due to the 17.6 Mev component.

The CsBr($\gamma$,p) spectrum was corrected for loss assuming isotropic angular distributions and the range-energy relations of figure 6.5. In a similar manner, the NaI(Tl) spectrum was corrected using the data of Ophel (Wr 58).

After correcting for the molecular density of the two crystals and the 3.0 m.b. cross section for the $Cs^{133}(\gamma,p)$ reaction in this energy range (Wr 58), the cross section for the emission of photo-protons from $Br^{79,81}$ of energy greater than 6.5 Mev was found to be $3.3 \pm 0.5$ m.b.

2.8. Discussion.

The investigation of the photodisintegration of CsBr(Tl) using separated isotopes of bromine in the crystal would simplify the interpretation of the energy distributions considerably but attempts to obtain this type of scintillator have not been successful. The general features of the proton distribution in $Br^{79,81}(\gamma,p)Se^{78,80}$ are of some significance.

The Proton Evaporation Spectrum.

The energy distribution of photo-protons evaporated from a compound nucleus has been calculated for silver and bromine by Waffler (Wa 53) and are included in figure 7.6. A level density $w \propto \exp.(aE)^{1/2}$ and a nuclear radius $R = r_o A^{1/3}$ have been used†.

The evaporation spectrum is not significantly different for silver or bromine and we may compare these calculations with figure 7.3 to discuss the $Br^{79,81}(\gamma,p)$ spectrum. It is apparent in this reaction that the evaporation spectrum cannot account for all of the yield of protons above 8 Mev and it is concluded that both compound nucleus and direct photodisintegration are

---

† In figure 7.6, the values $r_o = 1.3.10^{-13}$cm. and $r_o = 1.5.\ 10^{-13}$cm. have been used with $a = A/5$, $(w_1)$ and $a = 1.6\ (A-40)^{1/2}$, $(w_2)$.

present. This has been observed in other medium elements (Hi 47, Di 50, By 51) at this gamma ray energy where compound nucleus formation has been the principal mechanism with some admixture of direct transitions.

3. Further Work.

It appears that a general extension of the use of inorganic scintillators as target detectors in photo-disintegration studies would be limited by the energy resolution of the particular scintillator and the number of isotopes in the crystal. The most spectacular results in this method have involved the good scintillators: NaI(Tl), KI(Tl), LiI(Eu) and CsI(Tl).

The recent development of techniques for selecting monochromatic gamma radiation from electron linear accelerators (Tz 57) would allow the use of these scintillators in the measurement over a wide energy range of excitation functions of the particle groups observed.

A method has recently been devised for discriminating between alpha, proton and electron pulses in organic and inorganic scintillators (Ow 59) and this may overcome the problem of the electron background, allowing the use of larger scintillators with weaker monochromatic gamma ray sources such as $F^{19}(p;\alpha,\gamma)$, $B^{11}(p,\gamma)C^{12}$ and $H^{3}(p,\gamma)He^{4}$. It would also be possible to measure $(\gamma,\alpha)$ reactions by this method and to measure

photo-protons from thin foils placed over larger scintillators. Organic scintillators would be more attractive detectors because of the high threshold for the $C^{12}(\gamma,p)$ reaction.

# CHAPTER VIII.

## A Preliminary Investigation of the $Ne^{21}(d,p)Ne^{22}$ Reaction.

Introduction.

Particle-induced reactions (apart from stripping reactions), like photonuclear reactions, might be expected to proceed either by a compound nucleus or a direct process. It would be of interest to compare the $(\gamma,p)$ reactions measured in thin, inorganic scintillators with a series of particle-induced reactions which lead to proton transitions in the same residual nucleus, especially where the same excitation energy is involved in the reactions. For example, the $Na^{23}(\gamma,p)Ne^{22}$ reaction could be compared with the $Ne^{21}(d,p)Ne^{22}$ reaction at $E_d$ = 760 Kev and the $F^{19}(\alpha,p)Ne^{22}$ reaction at $E_\alpha$ = 8.4 Mev.

For a detailed comparison of the several reactions leading to proton transitions to the same residual nucleus, one would require a knowledge of the energy spectra and the angular distribution of each transition.

Many of the possible reactions are beyond the energy range of the accelerating machines at present available in this laboratory but the following chapter describes an attempt to study the $Ne^{21}(d,p)$ reaction at 760 Kev. Earlier workers † have only observed proton transitions to the ground and first excited states of

---

† Ambrosen,J. and Bisgaard, K.M., Nature 165, 888
Zucker,A and Watson, W.W. Phys. Rev. 78, 14.

$Ne^{22}$ and no angular distributions have been measured. The present investigation was attempted to see if one can identify in addition transitions by way of the levels of $N_e{}^{22}$ reported by Ophel and Wright (Op 58) at 5.4, 4.4 and 3.3 Mev in the $Na^{23}(\gamma,p)Ne^{22}$ reaction and to measure the angular distribution of each transition.

2. Preliminary Investigation.

1 $\mu$ gm./$_{cm.2}$ targets of $Ne^{21}$ absorbed in 0.0005 in. silver backing supplied by the electro-magnetic separator group at Harwell were mounted in the 90° target chamber shown in figure 6.2 and were bombarded with 760 Kev deuterons. As gas adsorbed on the silver backing leaves the target at temperatures above 200°C, the beam current was limited to 2$\mu$A and the target was water-cooled. The proton yield was observed with a $^3/_4$ in. x $^3/_4$ in. x 0.060 in. CsI(Tl) scintillation counter mounted on an E.M.I. photomultiplier type 6099F. A series of aluminium stopping foils mounted on the foil rack was used to assist in the identification of the proton groups in the spectrum and an energy calibration of the detector was made by observing the $B^{10}(d,p)B^{11}$ reaction in the manner described in chapter VI, section 4.2.

Proton groups from the $Ne^{21}$ target were observed at energies of 8.5, 6.5 and 3.2 Mev, corresponding to

(d,p) reactions in $N^{14}$, $C^{13}$ and $H^2$ respectively, but there was no evidence for proton groups from the $Ne^{21}$ (d,p)$Ne^{22}$ reaction. It was concluded that the deposit was too low to observe this reaction in competition with the contaminants in the target.

2.1. Target Preparation.

Attention was then given to the estimation of the minimum target thickness required to measure the $Ne^{21}$(d,p)$Ne^{22}$ reaction at this bombarding energy and to see what limits could be placed on the carbon and nitrogen contamination of the target surface. The investigation was carried out using natural neon gas, which is 90.9% $Ne^{20}$, assuming the $Ne^{21}$(d,p) cross section to be comparable with that of $Ne^{20}$(d,p).

To reduce the contaminants in the 0.005 in. thick silver backing used in the deposition, it was polished with fine abrasive paste and outgassed by heating it to a dull red heat in vacuo for a few minutes. The clean foil was mounted on a water-cooled probe in the 1.2 Mev accelerator immediately above the 90° analysing magnet. Natural neon gas was fed to the ion source and the foil was bombarded with 100μA. of neon ions at 300 Kev for two hours. In this time, the target thickness would have been 10 mg./$_{cm.2}$ if all the ions were absorbed on the silver - which is not the case since the surface

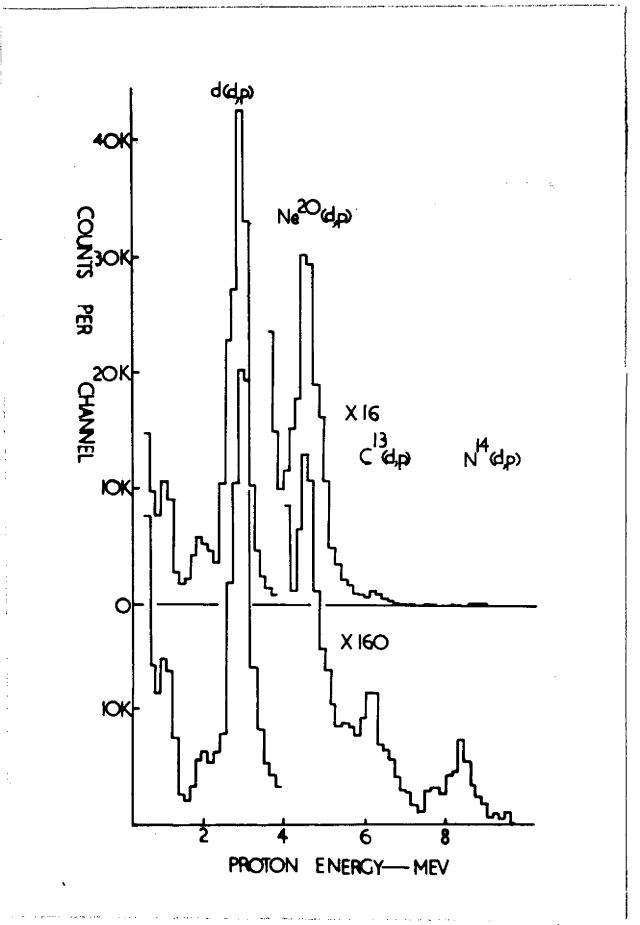


Fig. 8.1. Spectra observed through a 3 mg./$_{cm.^2}$ aluminium foil from the deuteron bombardment of $Ne^{20}$ adsorbed on silver backings($E_d$ = 760 Kev).

Upper Spectrum: Target prepared in this laboratory.

Lower Spectrum: 10 μgm./$_{cm.^2}$ target prepared in Harwell E.M. separator.

eventually becomes saturated with ions.[†] During the deposition, hot water was circulated through the probe in order to limit the deposition of carbon on the foil and to keep the temperature of the silver backing below 200°C.

A second target of $Ne^{20}$ adsorbed in silver was obtained from Harwell. This was deposited in an electromagnetic separator with an ion energy of 30Kev and it was believed to be saturated with a deposit of 10μ gm./$_{cm.2}$ $Ne^{20}$.

The two targets were bombarded with 760 Kev deuterons in the 90° target chamber and the spectra are compared in figure 8.1 after normalising to the same number of current integrator counts.

The peak at 4.5 Mev in both spectra corresponds to proton transitions in the $Ne^{20}(d,p)Ne^{21}$ reaction to the first excited state of $Ne^{21}$ at 0.35 Mev. (Aj 59). Ground state transitions were not resolved. The proton groups at 4.5 Mev are in the ratio of 10:1 and it was estimated that the deposit on the target prepared in this laboratory was 100 μ gm./$_{cm.2}$ and the target was saturated.

---

[†] Koch, J. " Electromagnetic Isotope Separators " North-Holland, Amsterdam, 1958.

It appears that the higher ion energy used in this deposition allows a deeper penetration of the silver backing and consequently, thicker targets can be prepared.

The carbon and nitrogen contamination of the backing material prepared in this laboratory is not significantly different from the commercial target.

It appears that the minimum target thickness required to investigate the $Ne^{21}(d,p)Ne^{22}$ reaction would be of the order of 10 $\mu$ gm./$_{cm.2}$ $Ne^{21}$. Thicker $Ne^{21}$ targets could be prepared in this laboratory but because of the low abundance of this isotope (0.28%), enrichment of natural neon by thermal diffusion is a lengthy process and supplies of the enriched gas are rare.

2.2. Further Investigation.

$Ne^{21}$ targets deposited on 0.0005 in. silver backing were obtained from the Laboratory of Mass Spectrography in Amsterdam. They were prepared in an E.-M. separator with an ion energy of 20 Kev and were believed to saturate at 10 $\mu$ gm./$_{cm.2}$. Because of the presence of $Ne^{20}H$ ions which are deposited with $Ne^{21}$, the targets were estimated to be 35% $Ne^{21}$ (P.K. Rol, private communication).

Figure 8.2 shows the proton spectrum from the bombardment of this target with 760 Kev deuterons. The spectrum was obtained using the 90° target chamber shown

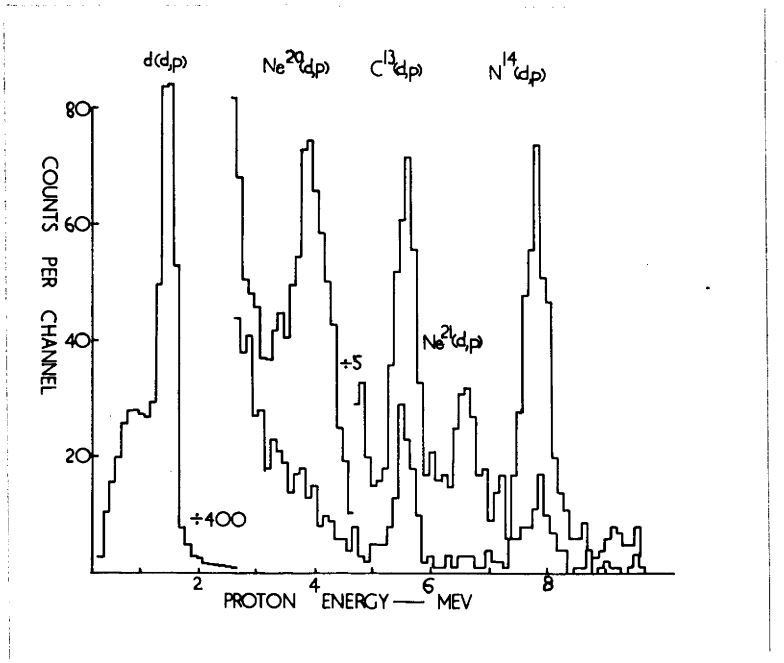


Fig. 8.2. Spectra observed through a 13 mg./cm.$^2$ aluminium foil from the deuteron bombardment of a neon target prepared in the Amsterdam E.M. separator (approx. 10 μgm./cm.$^2$ $Ne^{20}$ + 35% $Ne^{21}$). The lower spectrum was obtained by bombarding the reverse side of the target.

in figure 6.2 with a 13 mg./$_{cm.2}$ aluminium foil between the target and detector. The lower spectrum was obtained by bombarding the reverse side of the target and the energy scale is from a comparison with the $B^{10}(d,p)B^{11}$ reaction in the manner described in chapter VI, section 4.2.

The groups at 7.8, 5.6 and 1.7 Mev which are common to both spectra correspond to (d,p) reactions in $N^{14}$, $C^{13}$ and $H^{2}$. The groups about 4 Mev are believed to be due to transitions to the ground and first excited states of $Ne^{21}$ in the $Ne^{20}(d,p)Ne^{21}$ reaction.and the group at 6.6 Mev corresponds to transitions to the first excited state of $Ne^{22}$ in the $Ne^{21}(d,p)Ne^{22}$ reaction.

Clearly a thicker $Ne^{21}$ target is required before transitions to the levels of $Ne^{22}$ at 5.4, 4.4, 3.3 and 0 Mev can be identified in the presence of so many competitive reactions.

## REFERENCES.


Aj 59. Ajzenberg,F. and Lauritsen,T.
Nuc. Phys. 11 , 1.

Ar 50. Argo,A.V., Gittings,H.T., Hemmendinger,A., and Tascheck,R.F.
Phys. Rev. 78 , 691.

Ar 51 . Aron,W.A, Hoffman,B.G. and Williams, F.C.
A.E.C.U.Report 663.

Ba 52. Barnes,C.A., Carver,J.H., Stafford,G.H, and Wilkinson,D.H.
Phys. Rev. 86, 359.

Be 37. Bethe,H.A. Rev. Mod. Phys. 9, 177.

Be 55. Bell,P.R., Davis,R.C. and Bernstein,W.
Rev. Sci. Inst. 26, 726.

Be 56. Berger,M.J. and Doggett,J.
J. Res. N.B.S. 56, 355.

Bl 52a. Blatt,J.M. and Weisskopf,V.F.
"Theoretical Nuclear Physics,"
John Wiley and Sons, 1952.

Bl 52. Blatt,J.M. and Biedenharn,L.C.
Rev. Mod. Phys. 24, 258.

Bo 48. Bonner,T.W. and Evans,J.E.
Phys. Rev. 73, 666.

Bo 56. Boyle,A.J.F. Nuc. Phys. 1, 581.

Br 60. Bradford,E. and Barker,F.
Private Communication.

Bu 50. Burcham,W. and Freeman,J.M.
Phil. Mag. 41, 921.

By 51. Byerly,P.R. and Stephens,W.E.
Phys. Rev. 83, 54.

Ca 55. Carver,J.H., Hay,H.J. and Titterton,E.W.
Phil. Mag. 46, 841.

Ca 56. Campbell,J.G., Aust. J. Phys. 9, 156.

Ca 57. Carver,J.H., Edge,R.D., and Lokan,K.H.
Proc. Phys. Soc. A70, 415.

Ch 48. Christy,R.F. and Latter,R.
Rev. Mod. Phys. 20, 185.

Ch 53. Christy, R.F. Phys. Rev. 89, 839.

Co 49. Cohen,E.R. Phys. Rev. 75, 1463.

Da 55. Davisson,C.M. "Beta and Gamma Ray Spectroscopy." North-Holland, 1955.

De 49. Devons,S. and Hine,M.G.N.
Proc. Roy. Soc. A199, 56, 73.

De 50. Devons,S. and Lindsey,G.R.
Proc. Phys. Soc. A63, 1202.

De 54. Devons,S. and Goldring,G.
Proc. Phys. Soc. A67, 413.

De 57. Devons,S. and Goldfarb,L.J.B.
"Handbuch Der Physik" Vol XLII
Springer-Verlag 1957.

Di 50. Diven,B.C. and Almy,G.M.
Phys. Rev. 80, 407.

Ev 54. Evans,N.T.S. and Parkinson, W.C.
Proc. Phys. Soc. A67, 684.

Ev 55. Evans,R.D. "The Atomic Nucleus"
McGraw-Hill, 1957.

Fa 56. Fairstein,E. Rev. Sci. Inst. 27, 457.

Fl 51. Flowers,B.H. and Mandl,F.
Proc. Roy. Soc. A206, 131.

Fo 48. Fowler,W.A., Lauritsen,T and Lauritsen,C.C.
Rev. Mod. Phys. 20, 236.

Fo 49. Fowler,W.A. and Lauritsen,T.
Phys. Rev. 76, 314.

Fo 54. Foote,R.S. and Koch,H.W.
Rev. Sci. Inst. 25, 746.

Ga 51. Gaerttner,E.R. and Yeater, M.L.
Phys. Rev. 83, 146.

Ge 59. Gemmel,D.S., Morton,H. and Titterton,E.W.
Nuc. Phys. 10,39.

Ge 60. Gemmel,D.S. Aust.J. Phys., in the press.

Go 48. Goldhaber,M. and Teller,E.
Phys. Rev. 74, 1046.

Go 52. Goward,F.K. and Wilkins,J.J.
Proc. Roy. Soc. A217, 357.

Go 59a. Litherland,A.E., Paul,E.B., Bartholomew,G.A. and Gove,H.E. Phys. Rev. Letters 3, 177.
Can. J. Phys. 37, 53.
Phys. Rev. 114, 1312.

Go 59. Gove,H.E. "Nuclear Reactions" Vol.1. North-Holland, 1959.

Gr 48. Green,W.M. and Livesey,D.L.
Phil. Trans. Roy. Soc. 241, 323.

Gr 57. Grodstein,G.W.
N.B.S. Circular 583.

Ha 60. Hay,H.J. and Warren,J.B.
Can. J. Phys. 37, 1153.

Hi 47. Hirzell,O. and Waffler,H.
Helv. Phys. Acta. 20, 373.

Hu 40. Hudson,C.M., Herb,R.G. and Plain,G.J.
Phys. Rev. 57, 587.

In 54. Inall,E.K. and Boyle,A.J.F.
Phil. Mag. 44, 1081.

Jo 53. See Ge 60.

Ko 56. Koch,H.W. and Wyckoff,J.
J. Res. N.B.S. 56, 319.

Ko 59. Kockum,J. and Starfelt,N.
Nuc. Inst. 4, 171.

Kr 54. Kraus,A.A. Phys. Rev. 93, 1308.

Li 53. Liberman,D.A. and Christy,R.F.
Phys. Rev. 92, 1085A.

Li 55. Liberman,D.A. Ph.D. Thesis Caltech., 1955.

Lo 59. Lokan,K.H. Proc. Phys. Soc. 73, 697.

McD 47. McDaniel,B.D., von Dardel,G. and Walker,R.L.
Phys. Rev. 72, 985.

Ma 56. Mann,A.K., and Titterton,E.W.
Proc. Phys. Soc. A69, 917.

Ma 57. Mann,A.K.et.al. Bull. Am. Phys. Soc. 2, 181A.

Mi 56. Miller et.al. A.N.L. Report 5902.

Mo 53. Montalbetti,R., Katz,L. and Goldemberg,J.
Phys. Rev. 91,659.

Mu 52. Muller,R. and Stoll,P.
Nuovo Cimento. 9, 1232.

Na 51. Nabholtz,H., Stoll,P. and Waffler,H.
Phys. Rev. 82, 963.

Na 52. Nabholtz,H., Stoll,P. and Waffler,H.
Helv. Phys. Acta. 25, 153.

Na 52a. Nabholtz,H., Stoll,P. and Waffler,H.
Helv. Phys. Acta. 25, 701.

Ne 58. Neuert,H. and Retz-Schmidt,T.
Zeits. fur. Natur. 13a, 829.

Ne 57. Newson,H.W.: Williamson,R.M., Jones,K.W., Gibbons,J.H. and Marshak,H.
Phys. Rev. 108, 1294.

Op 58. Ophel,T.R. and Wright,I.F.
Proc. Phys. Soc. 71, 389.

Op 59. Ophel,T.R. Proc. Phys. Soc. A72, 321.

Ow 59. Owen,R.B. Nucleonics. 17, No.9, 92.

Pe 55. Perry,J.E. and Barne,S.J.
Phys. Rev. 99, 1368.

Ph 50. Phillips,J.A., Lawson,J.S. and Kruger,P.G.
Phys. Rev. 80, 326.

Pr 54. Price,P.C. Proc. Phys. Soc. A67, 849.

Ro 53. Rose,M.E. Phys. Rev. 91, 610.

St 51. Stearns,M.B. and McDaniel,B.D.
Phys. Rev. 82, 450.

St 53. Strauch,K. Ann. Rev. Nuc. Sci. Vol.2.

St 58. Strominger,D., Hollander,J.M. and Seaborg,G.T.
Rev. Mod. Phys. 30, 585.

St 58a. Storey,R.S., Jack,W. and Ward,A.
Proc. Phys. Soc. 72, 1, 1958.

Sw 55. Swann,C.P., Rothman,M.A., Porter,W.C. and Mandeville,C.E.
Phys. Rev. 98, 1183A

Ta 46. Tangen,R. K. Norske. Vidensk. Selsk. Skr. No.1.

Ti 53. Titterton,E.W. Aust. J. Sci. 15, 174.

Ti 54. Titterton,E.W. Phys. Rev. 94, 206.

Ti 55. Titterton,E.W. Prog. Nuc. Phys. Vol. 4.

To 51. Toms,M.E. and Stephens,W.E. Phys. Rev. 82, 709.

Tz 57. Tzara, C. Compt. Rend. 245, 56.

Vo 59. Vogt,E. "Nuclear Reactions," Vol.1. North-Holland 1959.

Wa 48. Walker,R.L. and McDaniel,B.D. Phys. Rev. 74, 315.

Wa 53a. Waters,W.D., Fowler,W.A. and Lauritsen,C.C. Phys. Rev. 91, 917.

Wa 53. Waffler,H. Helv. Phys. Acta. 26, 785.

We 51. Weisskopf,V.F. Phys. Rev. 83, 1073L.

Wi 51. Wilkinson,D.H. and Carver,J.H. Phys. Rev. 83, 466.

Wi 54. Wilkinson,D.H. Phil. Mag. 45, 259.

Wi 56. Wilkinson,D.H. Physica 22, 1039.

Wi 59. Wilkinson, D.H. and Bloom: S.D.
Phys. Rev. 105, 683.
Tanner, N.W., Thomas, G.C. and Meyerhof,W.E.
Nuovo Cimento 14, 257.

Wr 57. Wright,I.F., Morrison,D.R.O., Reid,J.M.
and Atkinson,J.R.
Proc. Phys. Soc. A69, 77.

Wr 58. Wright,I.F. Private Communication.

Ya 48. Yang,C.N. Phys. Rev. 74, 764.